Tectonics®

RESEARCH ARTICLE
10.1029/2024TC008340

Key Points:

- Polyphase extensional, compressional, and strike-slip deformation in the Northern Andes Central Cordillera
- A geo- and thermochronological approach unravels the detailed deformation history of the Northern Andes
- Relations between exhumation, hydrothermal activity, and rock metamorphism during basement reworking

Supporting Information:

Supporting Information may be found in the online version of this article.

Correspondence to:

S. Zapata,
sebastian.zapatah@urosario.edu.co

Citation:

Zapata, S., Cardona, A., Jaramillo-Ríos, J. S., Siachoque, A., Peverelli, V., Chew, D., et al. (2024). Repeated structural reworking in the basement of the Central Colombian Andes unraveled by a multi-chronometric approach. *Tectonics*, *43*, e2024TC008340. https://doi.org/10.1029/2024TC008340

Received 19 MAR 2024
Accepted 1 OCT 2024

Author Contributions:

Conceptualization: S. Zapata, A. Cardona
Data curation: J. S. Jaramillo-Ríos, V. A. Valencia
Formal analysis: V. Peverelli, D. Chew, E. R. Sobel, L. C. Calderon-Diaz, V. A. Valencia, A. M. Patiño, J. Glodny
Funding acquisition: S. Zapata, A. Cardona
Investigation: S. Zapata, A. Cardona, A. Siachoque, V. Peverelli, K. Wemmer, M. C. Rodríguez, J. C. Valencia-Gomez, L. C. Calderon-Diaz
Methodology: S. Zapata, J. S. Jaramillo-Ríos, V. Peverelli, E. R. Sobel, V. A. Valencia, J. Glodny
Project administration: S. Zapata, A. Cardona, M. Parra, G. E. Botello
Supervision: A. Cardona
Writing – original draft: S. Zapata, A. Cardona
Writing – review & editing: S. Zapata, A. Cardona, J. S. Jaramillo-Ríos,

Repeated Structural Reworking in the Basement of the Central Colombian Andes Unraveled by a Multi-Chronometric Approach

S. Zapata[1], A. Cardona[2], J. S. Jaramillo-Ríos[2], A. Siachoque[2], V. Peverelli[3], D. Chew[4], K. Wemmer[5], M. C. Rodríguez[2], J. C. Valencia-Gomez[2], E. R. Sobel[6], L. C. Calderon-Diaz[1], V. A. Valencia[7], A. M. Patiño[8], M. Parra[8], G. E. Botello[2], and J. Glodny[9]

[1]Faculty of Natural Sciences, Grupo EGEO, Universidad del Rosario, Bogotá, Colombia, [2]Facultad de Minas, Grupo EGEO, Universidad Nacional de Colombia, Medellín, Colombia, [3]Institute of Geological Sciences, University of Bern, Bern, Switzerland, [4]Department of Geology, School of Natural Sciences, Trinity College Dublin, Dublin, Ireland, [5]Geowissenschaftliches Zentrum, Georg–August–Universität, Göttingen, Germany, [6]Institute of Geosciences, University of Potsdam, Potsdam, Germany, [7]School of Earth and Environmental Science, Washington State University, Pullman, WA, USA, [8]Institute of Geosciences, University of Sao Paulo, São Paulo, Brazil, [9]GFZ German Research Centre for Geosciences, Potsdam, Germany

Abstract Long-lived orogens are often characterized by basement blocks affected by polyphase thick-skinned deformation. Deciphering these events is challenging due to the heterogeneous and complex structural histories resulting from the superposition of multiple deformation phases. For instance, the Central Cordillera of Colombia was shaped by multiple tectonic phases during the Mesozoic and Cenozoic, which have been poorly constrained in both space and time. To unravel the deformation history of this mountain belt, we conducted field mapping and applied a multi-chronometric approach that included zircon and apatite U-Pb dating of the igneous basement, epidote and titanite U-Pb dating of structurally controlled mineralization events, K-Ar dating of fault rock illite, and fission track and (U-Th-Sm)/He bedrock thermochronology of apatite and zircon. The results reveal six deformation events along two fault systems during the past 184 Myr. This deformation history started in the Jurassic with structurally controlled magmatism and ductile deformation; followed by brittle-ductile and fluid-assisted basin subsidence and inversion during the Cretaceous. Finally, the Cenozoic was characterized by brittle strike-slip and compressional deformation. Our findings show the basement response to polyphase reworking, highlighting the prominent role of ancient upper-plate discontinuities, magmatism, and fluids.

1. Introduction

Deciphering long-term deformation histories in basement rocks has far-reaching implications for our understanding of orogenic processes (Holdsworth, Hand, et al., 2001; Nuriel et al., 2019). In long-lived continental margins, prolonged polyphase deformation reworks the basement, leading to the nucleation and development of faults along preexisting heterogeneities, structurally controlled magmatic and hydrothermal activity, fault-related metamorphism, and rock exhumation and uplift (e.g., Butler et al., 2008; Holdsworth, Stewart, et al., 2001; Horton & Folguera, 2022; Peverelli, Berger, Mulch, et al., 2022). However, these effects on basement rocks are often investigated separately and can be overprinted during subsequent deformation, preventing a comprehensive understanding of the relationships among the processes that characterize continental basement reworking and their role in orogenic growth.

Retrieving deformation events from basement rocks in polyphase orogens can be challenging due to the superposition of these events, the scarcity of synorogenic rocks, discrete exposures of newly formed structures, and the absence of a complete structural record amenable to geochronology (e.g., Mottram et al., 2020; Tsukamoto et al., 2020). Therefore, orogenic phases are often constrained by indirect deformational proxies such as sedimentary routing systems and their provenance, and rock cooling histories (e.g., Fitz-Diaz & van der Pluijm, 2013; Horton et al., 2020; Pearson et al., 2013). However, in recent years, the refinement and development of geochronometric techniques applied to minerals formed in structural fabrics (e.g., Ceccato et al., 2024; Hueck et al., 2022) or during structurally controlled hydrothermal precipitation (e.g., epidote, titanite, apatite, and calcite) have provided new possibilities for the reconstruction of basement deformation phases (Hueck et al., 2022; Kirkland et al., 2018; Peverelli et al., 2021). Therefore, studying mineral and isotopic products of

A. Siachoque, V. Peverelli, D. Chew, K. Wemmer, M. C. Rodríguez, J. C. Valencia-Gomez, E. R. Sobel, A. M. Patiño, M. Parra, G. E. Botello, J. Glodny

basement deformation using traditional and recently developed geo- and thermochronological techniques can provide detailed deformation histories.

The development of the Northern Andes is the result of protracted deformation that caused the vertical and lateral juxtaposition of pre-orogenic crustal blocks—a geological configuration that led to contrasting and/or incomplete paleogeographic and tectonic reconstructions (e.g., Montes et al., 2019; Mora et al., 2020; Restrepo-Moreno et al., 2019; Zapata et al., 2021). The Central Cordillera of Colombia, located within the central segment of this orogen, is an NNE mountain belt that is mostly composed of pre-Cenozoic crystalline basement exhumed and uplifted during several Mesozoic to Cenozoic deformational phases that followed an older Early Cretaceous extensional setting (Calderón-Díaz et al., 2023; Noriega-Londoño et al., 2020; Restrepo-Moreno et al., 2009; Villagómez & Spikings, 2013; Villamizar-Escalante et al., 2021; Zapata et al., 2020, 2021).

Current reconstructions of the Central Cordillera's evolution encompass a poorly understood Jurassic deformational and metamorphic history (Bayona, Bustamante, et al., 2020; Blanco-Quintero et al., 2014); the development of Early Cretaceous extensional basins that underwent inversion during the Late Cretaceous (Calderón-Díaz et al., 2023; Nivia et al., 2006; Villagómez & Spikings, 2013; Zapata et al., 2019); and a diverse array of Paleogene tectonic settings comprising strike-slip, compressional, and extensional deformation (Jaramillo et al., 2022; Villamizar-Escalante et al., 2021). Furthermore, several studies have proposed distinct patterns of Neogene uplift and exhumation along the Central Cordillera (Noriega-Londoño et al., 2020; Ott et al., 2023; Pérez-Consuegra et al., 2021). This deformation history has been related to the activity of several NNE faults bounding Central Cordillera (e.g., Cauca-Romeral and Chusma fault systems) and NW and NE fault systems (e.g., Paez, Ibague, and Espiritu Santo fault systems) that segmented and deformed this mountain belt.

The structural blocks comprising the Central Cordillera exhibit notable variations in the proposed magnitude, timing, and spatial extent of deformation (Noriega Londoño, 2016; Ott et al., 2023; Villamizar-Escalante et al., 2021; Zapata et al., 2021). These differences are related to their distinct structural evolution and the varied methodological approaches employed to analyze deformation, highlighting the need for detailed multi-technique studies. Furthermore, the effects and chronological sequence of these deformation events within the crystalline basement of the Central Cordillera, and their relationships with major fault systems, remain poorly understood. Specifically, in the southeastern segment of the Central Cordillera, the pre-Cenozoic basement evolution, the timing of basin inversion, and the magnitude of Cenozoic deformation are open research questions.

Permian and Jurassic igneous rocks in the southern segment of the Central Cordillera (Figure 1) display evidence of structurally controlled magmatism and hydrothermal activity, along with ductile-brittle deformation, as shown by mylonites, breccias, and gouges related to different fault systems (Rodríguez-Cuevas et al., 2024). These deformational features within these plutonic rocks provide a unique opportunity to employ traditional and more recently developed geo- and thermo-chronological techniques to resolve the polyphase deformational history of the Central Cordillera.

In this contribution, we present a multi-chronometric study of the southern Central Cordillera, including zircon and apatite U-Pb geochronological data to constrain the time of magma emplacement and post-magmatic cooling (e.g., Kent & Cooper, 2018; Kirkland et al., 2018) while epidote and titanite U-Pb dating were employed to reconstruct fracture and vein-filling, and hydrothermal alteration events (Moser et al., 2022; Peverelli, Berger, Mulch, et al., 2022, 2023). Additionally, modeled low-temperature thermochronological data were used to reveal the basement thermal history (Reiners & Brandon, 2006). Finally, illite K-Ar age data and complementary X-ray diffractometry (XRD) data were undertaken on fault rocks to yield direct insights into the timing and temperature conditions of basement deformation (e.g., Hueck et al., 2020).

The results are used to present a detailed and complete Jurassic to Pliocene deformation history of the southern Central Cordillera. This tectonic evolution history underscores the wide array of deformational processes that modify the basement during the evolution of long-lived continental margins, including rock uplift and exhumation, basin subsidence and reheating, syn-deformational hydrothermal activity, and brittle to brittle-ductile basement deformation. The high level of detail provided by our study argues that multi-methodological approaches are essential for unraveling complex basement deformation histories.

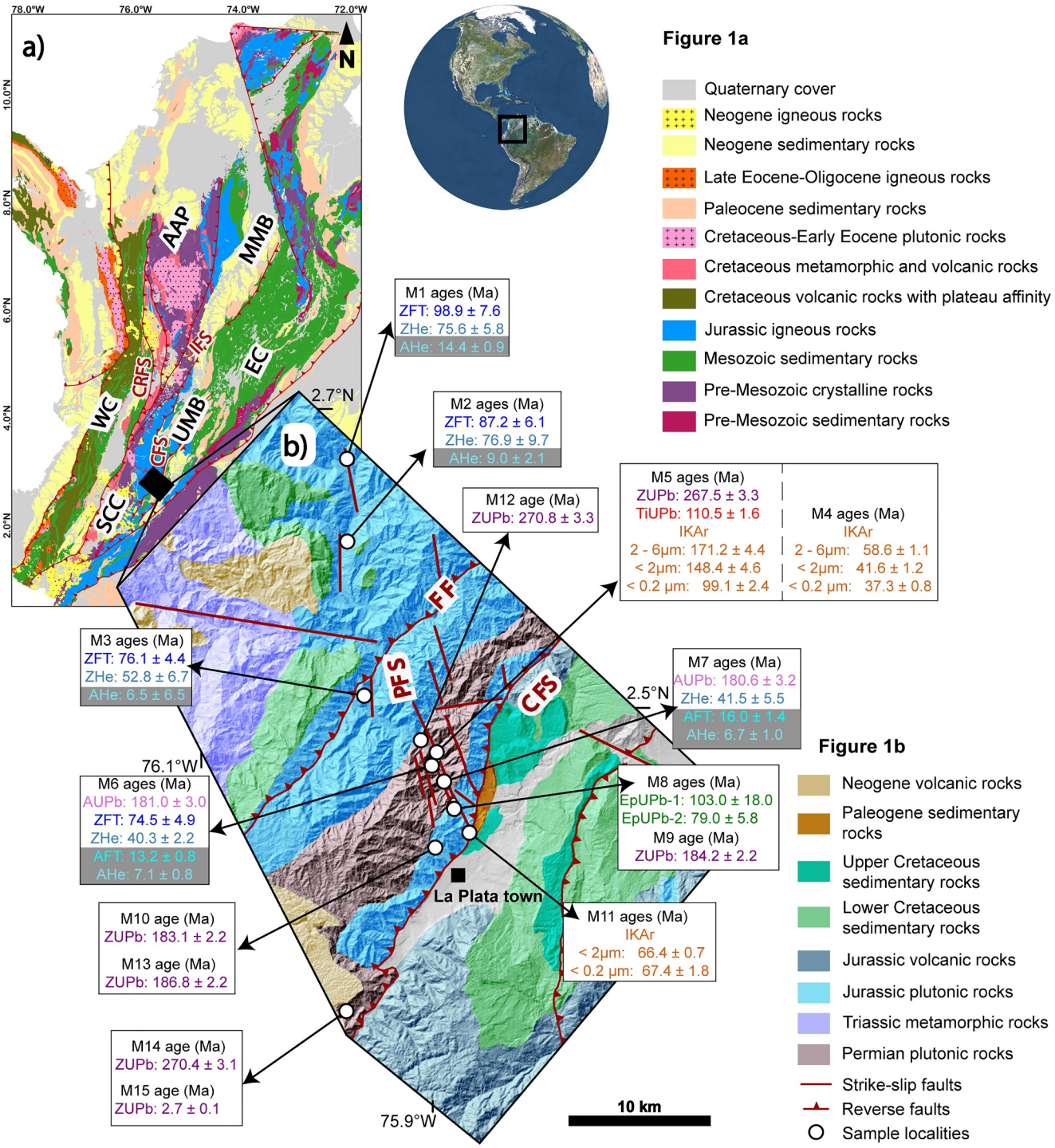

Figure 1. (a) Geological map of the Colombian Andes; WC, Western Cordillera; AAP, Antioquia Altiplano Province; SCC, Southern Central Cordillera; EC, Eastern Cordillera; UMB, Upper Magdalena Basin; MMB, Middle Magdalena Basin; CFS, Chusma Fault System; IFS, Ibague Fault System; CRFS, Cauca-Romeral Fault System. (b) Geological map of the study area; PFS, Paez Fault System; CFS, Chusma Fault System; FF, Frailes Fault; white circles indicate the collected samples while the sample codes and the obtained geo- and thermochronological ages are presented in the outside boxes. ZUPb, zircon uranium-lead; AUPb, apatite uranium-lead; EpUPb, epidote uranium-lead; TiUPb, Titanite uranium-lead; IKAr, illite potassium-argon; AFT, apatite fission track; ZFT, zircon fission track; AHe, apatite uranium-thorium/helium; ZHe, zircon uranium-thorium/helium.

2. Tectonic Evolution of the Central Cordillera and the Upper Magdalena Basin

The Colombian Andes encompass three distinct mountain belts distinguished by their contrasting tectonic evolution (Figure 1a). The Central Cordillera is characterized by a pre-Cretaceous crystalline basement that underwent deformation and exhumation between the Jurassic and the Pliocene (Spikings et al., 2015). In contrast, the Eastern and Western cordilleras exhibit different basement rocks and a deformation history restricted to the Cenozoic. The Eastern Cordillera mostly consists of sedimentary rocks that accumulated in Paleozoic to Paleogene basins that were widely inverted during the Cenozoic (Costantino et al., 2021; Horton et al., 2020; Mora et al., 2006). In contrast, the Western Cordillera consists of Cretaceous oceanic, volcanic, and sedimentary rocks that formed allochthonous to the continental margin, as part of the Caribbean Plateau (Hincapié-Gómez et al., 2018; Kerr & Tarney, 2005). These rocks were intruded by arc-related plutons and accreted to the continental margin during the Late Cretaceous (Spikings et al., 2015).

The Central Cordillera predominantly comprises pre-Cenozoic igneous and metamorphic rocks that underwent a polyphasic deformation history (Noriega-Londoño et al., 2020; Restrepo-Moreno et al., 2009; Villamizar-Escalante et al., 2021; Zapata et al., 2020, 2021). The basement of the Central Cordillera is cut by several NW- and NE- striking fault systems, such as the Ibagué, Paez, and Espiritu Santo fault systems (Figure 1a). Variations in basement composition, exhumation, and mountain belt morphology have been linked to distinct along-strike tectonic and deformational histories in the northern and southern segments of the Central Cordillera, which are separated by the Ibagué Fault System (Ott et al., 2023; Pérez-Consuegra et al., 2021). Major NNE-striking fault systems are parallel to the trend of this mountain belt and represent the limit between the Central Cordillera basement and adjacent basins. The Cauca-Romeral Fault System separates the Central Cordillera from the Cenozoic Cauca Basin and the accreted oceanic terranes in the west, while the Chusma Fault System is the limit with the Upper Magdalena Jurassic to Cenozoic strata (Figure 1a) (Kammer & Bermúdez, 2013; Rodríguez-Cuevas et al., 2024; Vinasco & Cordani, 2012).

Available regional tectonic models for the tectonic evolution of the Central Cordillera rely on its thermochronological and magmatic record, the analysis of sedimentary strata within adjacent basins, and limited geochronological constraints related to basement metamorphism (e.g., Bayona et al., 2012; Blanco-Quintero et al., 2014; Pardo-Trujillo et al., 2020; Villamizar-Escalante et al., 2021; Zapata et al., 2021).

In the southern segment of the Central Cordillera, the basement mostly consists of Jurassic rocks intruding Permian plutonic and Triassic metamorphic rocks, while the basement of the adjacent Upper Magdalena Basin consists of Jurassic volcanic and plutonic rocks (Figure 1) (Bustamante et al., 2016; Rodríguez-Cuevas et al., 2024; Rodríguez–García et al., 2019). An unconformity separates the basements of the Central Cordillera and the Upper Magdalena Basin from Cretaceous strata deposited during extensional phases between ∼135 and 90 Ma (Calderón-Díaz et al., 2023; Valencia-Gómez et al., 2024).

The uplift of the Central Cordillera commenced around 90 Ma and intensified between 72 Ma and 62 Ma during the collision of the Caribbean Plateau with the continental margin (Cardona et al., 2020; Spikings et al., 2015; Zapata et al., 2021). These contractional events caused the inversion of some Early Cretaceous extensional basins and modified the regional sedimentary systems; in the Upper Magdalena Basin, Early Cretaceous shallow marine sedimentation transitioned to coarsening-up Late Cretaceous to Paleocene fluvial sedimentation (Bayona, 2018; Calderon-Diaz et al., 2024; Carvajal-Torres et al., 2022). The Paleocene paleogeography of the Northern Andes was characterized by the reinitiation of continental arc magmatism along the Central Cordillera and the development of alluvial and fluvial systems in response to the emergence of relatively high topography (Bayona, 2018; Bayona et al., 2013; Carvajal-Torres et al., 2022).

Multiple tectonic scenarios have been proposed for the evolution of distinct segments of the Central Cordillera between the Eocene and the Oligocene. The proposed models include: (a) relative tectonic quiescence marked by slow exhumation and subsidence rates (Reyes-Harker et al., 2015; Villamizar-Escalante et al., 2021; Zapata et al., 2021), (b) extensional tectonics (Kammer & Bermúdez, 2013), (c) regional strike-slip deformation (Jaramillo et al., 2022; Zapata et al., 2021), and (d) major rock uplift and exhumation during tectonic contraction (Montes et al., 2019). In the Upper Magdalena Basin, an Eocene unconformity separates the Cretaceous and Paleocene strata from the Oligocene coarse-grained alluvial sedimentation (Carvajal-Torres et al., 2022; Ramon & Rosero, 2006).

Major exhumation and uplift characterized the Colombian Andes after ~20 Ma (e.g., Costantino et al., 2021; Pérez-Consuegra et al., 2022; Restrepo-Moreno et al., 2019), as evidenced by coarsening up successions in adjacent basins, including the lacustrine and fluvial strata preserved in the Upper Magdalena Basin (Mora-Rojas et al., 2023; Ramon & Rosero, 2006; Zapata et al., 2023). In the northern segment of the Central Cordillera, also known as the Antioquia Altiplano Province (APP), present-day positive relief has been interpreted as the result of minor exhumation and relatively high surface uplift during the Miocene (Ott et al., 2023; Pérez-Consuegra et al., 2021; Zapata et al., 2021). In contrast, the relief in the southern segment of the Central Cordillera has been attributed to regional Miocene basement exhumation and surface uplift (Ramon & Rosero, 2006; Zapata et al., 2023).

The subduction history of the Nazca plate, including the Late Neogene flat slab event, the subduction of the Carnegie ridge, and the collision of the Panama block have been considered major triggers of the different Neogene orogenic phases (Mora et al., 2020; Pérez-Consuegra et al., 2021; Spikings & Simpson, 2014).

3. Analytical and Sampling Methods

Detailed field mapping and microstructural analysis were combined with multiple geo- and thermochronological data obtained from samples collected from the southeastern segment of the Central Cordillera (Figure 1a). U-Pb geochronology by inductively coupled plasma mass spectrometry (LA-ICP-MS) was applied to zircon, apatite, titanite, and epidote to place time constraints on magmatic crystallization, post-magmatic cooling, and structurally controlled mineralization (e.g., Bakker & Elburg, 2006; Chew & Spikings, 2021; Frost et al., 2001; Peverelli et al., 2021, 2023). Low-temperature thermochronology methods, including fission-tracks and (U-Th/He) techniques applied to both zircon and apatite were employed to reconstruct the thermal history of the studied region (Reiners & Brandon, 2006). Additionally, illite K-Ar geochronology was utilized to determine the direct age of rock deformation (Hueck et al., 2022). The details of sample collection and preparation are presented in Text S1 in Supporting Information S1.

3.1. Microstructural Analysis

A detailed petrographic analysis of the faulted rocks aimed to identify the textural relationships between neoformed minerals and deformation mechanisms in magmatic, sub-magmatic, and/or solid-state conditions. The analyses were carried out based on the microstructural criteria outlined by Stipp et al. (2002) and Passchier and Trouw (2005). The petrographic microtextural analysis was complemented by semi-quantitative energy-dispersive spectrometry analysis and back-scattered electron (BSE) imaging.

3.2. U-Pb Methods (Zircon, Apatite, Titanite, and Epidote)

U-Pb geochronology is based on quantification of the decay of ^{235}U to ^{207}Pb and ^{238}U to ^{206}Pb, following the isotope closure of a given U-bearing mineral system (Chang et al., 2006; Corfu, 2013). These two isotopic systems have different decay constants, offering the opportunity to obtain two ages for a single mineral phase, which can be used to double-check the obtained ages and to calculate ages without knowing the amount of initial lead incorporated by the mineral (Chew et al., 2014; Corfu, 2013).

The zircon U-Pb system has a closure temperature above 900°C (Lee et al., 1997); given that this mineral phase is highly resistant to either subsequent sedimentary transport or chemical alteration, it has the potential to preserve the age of high-temperature magmatic and metamorphic events, even when eroded into sedimentary systems (Gehrels, 2012). Moreover, the relatively low initial lead content that zircon can incorporate makes it a powerful and precise geochronometer.

In contrast, other mineral phases such as epidote, titanite, and apatite incorporate significant amounts of initial lead in their crystal structures, which represents an additional challenge compared to the zircon U-Pb dating method (Chew & Spikings, 2021; Peverelli et al., 2021; Schmitz & Bowring, 2001). The initial lead isotope composition needs to be inferred either from choosing an appropriate value, for example, by measuring U-free coexisting minerals, by employing crustal Pb evolution models, or by dating several grains inferred to be cogenetic. When plotting non-corrected $^{238}U/^{206}Pb$ versus $^{207}Pb/^{206}Pb$ isotopic ratios, cogenetic grains should distribute along a single line termed as isochron or regression, the intercept of this line with the $^{207}Pb/^{206}Pb$ axis represents the initial lead isotopic composition, while the slope is used to obtain the isochron age.

Titanite can be stable in a wide range of metamorphic and igneous facies, which together with its high closure temperature for the U-Pb system (>600°C) makes it an ideal geochronometer to date metamorphism or hydrothermal activity (Moser et al., 2022; Sun et al., 2012). Zircon and titanite U-Pb isotopes were measured at the Radiogenic Isotope and Geochronology Lab (RIGL) at Washington State University. Detailed laboratory procedures are presented in Text S2 in Supporting Information S1.

Apatite is a common accessory mineral found in igneous and metamorphic rocks. The apatite U-Pb system has closure temperatures between 450 and 550°C, making it suitable for reconstructing post-magmatic cooling histories or exhumation events (Chew & Spikings, 2021; Kirkland et al., 2018). Apatite U-Pb isotope and trace element data were obtained at the Department of Geology of the Trinity College in Dublin (Ireland). Detailed procedures are presented in Text S3 in Supporting Information S1.

Epidote-group minerals typically crystallize over a wide range of P-T conditions in diverse magmatic, metamorphic, and hydrothermal environments in continental and oceanic crusts (Bird & Spieler, 2004; Schmidt & Poli, 2004). Recent investigations have shown the reliability of epidote as a U-Pb geochronometer by using in situ quadrupole dating (LA-ICPMS) with magmatic allanite as reference material (Peverelli et al., 2021; Peverelli, Berger, Mulch, et al., 2022; Peverelli, Berger, Wille, et al., 2022). Due to the polyphase nature of hydrothermal alteration, epidote dating requires detailed textural analysis and in-situ dating to prove the existence of co-genetic suites of epidote crystals. U–Pb isotope analyses were performed at the University of Bern (Switzerland). Detailed procedures and parameters are provided in Text S4 and Table S1 in Supporting Information S1, detailed data is in Data Set S1.

All U-Pb ages are presented with the number of analyzed spots (*n*), the 2-sigma error, and the mean square weighted deviation (MSWD).

3.3. K-Ar Illite Dating and Illite Crystallinity (IC) Methods

Fault deformation results in increased temperature at the fault core, leading to fluid-assisted neoformation and the recrystallization of several minerals. Techniques such as potassium-argon (K-Ar) dating complemented by XRD data on authigenic illite can provide the direct timing and approximate temperature conditions for the formation of fault rocks such as mylonites, breccias, and gouges (Hueck et al., 2022; Stewart et al., 2000).

IC is defined as the peak width at half-height of the 10-Å peak. IC determinations are sensitive indicators of the degree of very low-grade metamorphism in clastic sediments (Jaboyedoff et al., 2001; Kralik et al., 1987; Kübler & Jaboyedoff, 2000).

For each sample three size fractions were analyzed: 60-2, <2, and <0.2 μm. Unfortunately, for sample M11, no K-Ar data was obtained for the coarser fraction due to the absence of illite. Moreover, for the finer fractions, IC data was not obtained because of the low resolution of the illite peak. Potassium-argon (K-Ar) dating and XRD analysis were performed at the Georg-August-Universität Göttingen. More detailed methods and procedures are presented in Text S5 in Supporting Information S1. The diffractometry patterns and detailed IC and K-Ar data are presented in Figure S1 and Tables S2 and S3 in Supporting Information S1, respectively.

3.4. Thermochronological Methods

Thermochronology is based on quantifying the time after the closure of a radioactive decay system, which can be inferred by measuring the radioactive parent isotopes and their radiogenic products (Dodson, 1973; Reiners & Zeitler, 2005). The retention of the radiogenic products occurs after the system cools below the closure temperature, which varies depending on cooling rates, mineral kinetic variability, and other conditions intrinsic to each system (Ehlers & Farley, 2003; Harrison, 2005).

3.4.1. Fission Tracks and (U-Th-Sm)/He Methods

The apatite (AFT) and zircon (ZFT) fission track methods are based on the spontaneous fission of ^{238}U which damages the crystal lattice (spontaneous fission tracks), providing information about the time passed since the first track was formed (Green et al., 1986; Wagner et al., 1989). Fission tracks in apatite can be partially annealed at temperatures between 60 and 120°C and fully annealed at higher temperatures; however, apatite resistance to annealing depends on mineral kinetics (Carlson et al., 1999; Green et al., 1986). The kinetics of fission tracks in

zircon are poorly known; however, closure temperatures in the range between 232 and 325°C have been estimated for naturally damaged and non-damaged zircons (Bernet, 2009; Ketcham, 2019; Reiners & Brandon, 2006). Analyses were carried out using the External Detector Method in the thermochronology laboratory and research center (CPGeo_LTC) of the University of Sao Paulo, Brazil (USP). Detailed procedures are presented in Text S6.1 in Supporting Information S1 and detailed data is available in Table S4 in Supporting Information S1.

Apatite (AHe) and zircon (ZHe) (U-Th-Sm)/He thermochronology quantify the production and accumulation of helium from the alpha decay of U, Th, and Sm. This method provides information on thermal histories between 100 and 40°C in apatite (Farley, 2002) and between 140 and 220°C in zircon. The helium in apatite and zircon is controlled by different factors including the cooling rate, the grain size, the composition as well as the effective uranium content (eU = U + 0.238*Th) (Brown et al., 2013; Flowers, 2009; Guenthner et al., 2013). For this study, possible eU or size controls were evaluated by revising positive or negative correlations between single-grain ages and the eU or equivalent spherical radius (ESR). In the absence of possible compositional or size controls, single-grain AHe and ZHe ages were considered reproducible when at least two-grain ages exhibit a 1σ standard deviation (S.D.) < 20% of the mean age (Flowers & Kelley, 2011). AHe and ZHe analyses were carried out at the Potsdam University (Germany) alphachron laboratory, while U, Th, Sm concentrations were measured at GFZ Potsdam. Detailed procedures are presented in Text S6.2 in Supporting Information S1 and detailed data is available in Table S5 in Supporting Information S1.

3.4.2. Modeling Approach

Interpreting thermal histories from multiple samples and methods can be challenging due to distinct kinetic models, data dispersion, and the presence of partially reset ages. These complexities can be mitigated through inverse thermal modeling, which integrates samples in various structural positions and incorporates kinetic models from each method to extract a thermal history model (Gallagher, 2012; Ketcham, 2005). This approach provides estimates of each time-temperature point and its associated confidence intervals. The QTQt software (V. 5.8.4) was used to model the thermochronological data. This software uses a Bayesian transdimensional statistical approach to obtain the most probable thermal history from multiple samples and multiple thermochronometers (Gallagher, 2012; Gallagher et al., 2009). We used the radiation damage models (RDAAM) from Flowers et al. (2009) and Guenthner et al. (2013) to predict the ages of the AHe and ZHe systems, respectively. The annealing model from Ketcham et al. (2007) was used to predict apatite fission track ages.

A high-temperature constraint was included in the model to represent the crystallization age of the Jurassic plutonic rocks. Although some of the samples were collected from a Permian roof pendant, fully reset Jurassic apatite U-Pb ages suggest temperatures above ~400°C during the intrusion of the Jurassic magmas, justifying this high-temperature constraint. A constraint to force the model to be close to surface temperatures between 140 and 100 Ma was also included; this constraint is based on the depositional ages of the overlying Cretaceous strata. Because accurate ZFT annealing models are not available (Bernet, 2009), ZFT data were not included in the model; instead, a constraint between 110 Ma and 90 Ma and between 232 and 325°C was set to represent reset ZFT data. The initial 250,000 iterations were discarded (burn-in) and the subsequent 250,000 were used to calculate the posterior probability (post-burn-in). The likelihood chain of the model is presented in Figure S2 in Supporting Information S1.

4. Results

In the following sections, we first present the geologic observations of the La Plata Block, followed by zircon U-Pb and low-temperature thermochronological data that is used to infer the crystallization age and the subsequent thermal evolution of the igneous host rocks (Figures 2 and 3). We then separate the structural, petrographic, and geochronological data based on their structural correlation with the CFS and PFS. The chronological data are summarized in Table 1.

4.1. Field Geologic Observations of the La Plata Block

In the eastern segment of the Southern Central Cordillera (Figure 1), the La Plata block is composed of La Plata Pluton, a Permian monzogranite, intruded by a Jurassic quartz-monzodiorite known as the Paez Pluton (Rodríguez–García et al., 2019). Both plutonic units are intruded by mafic dikes. These basement rocks of the La Plata Block are deformed by the NNE-striking Chusma and NW-trending Paez fault systems (CFS and PFS,

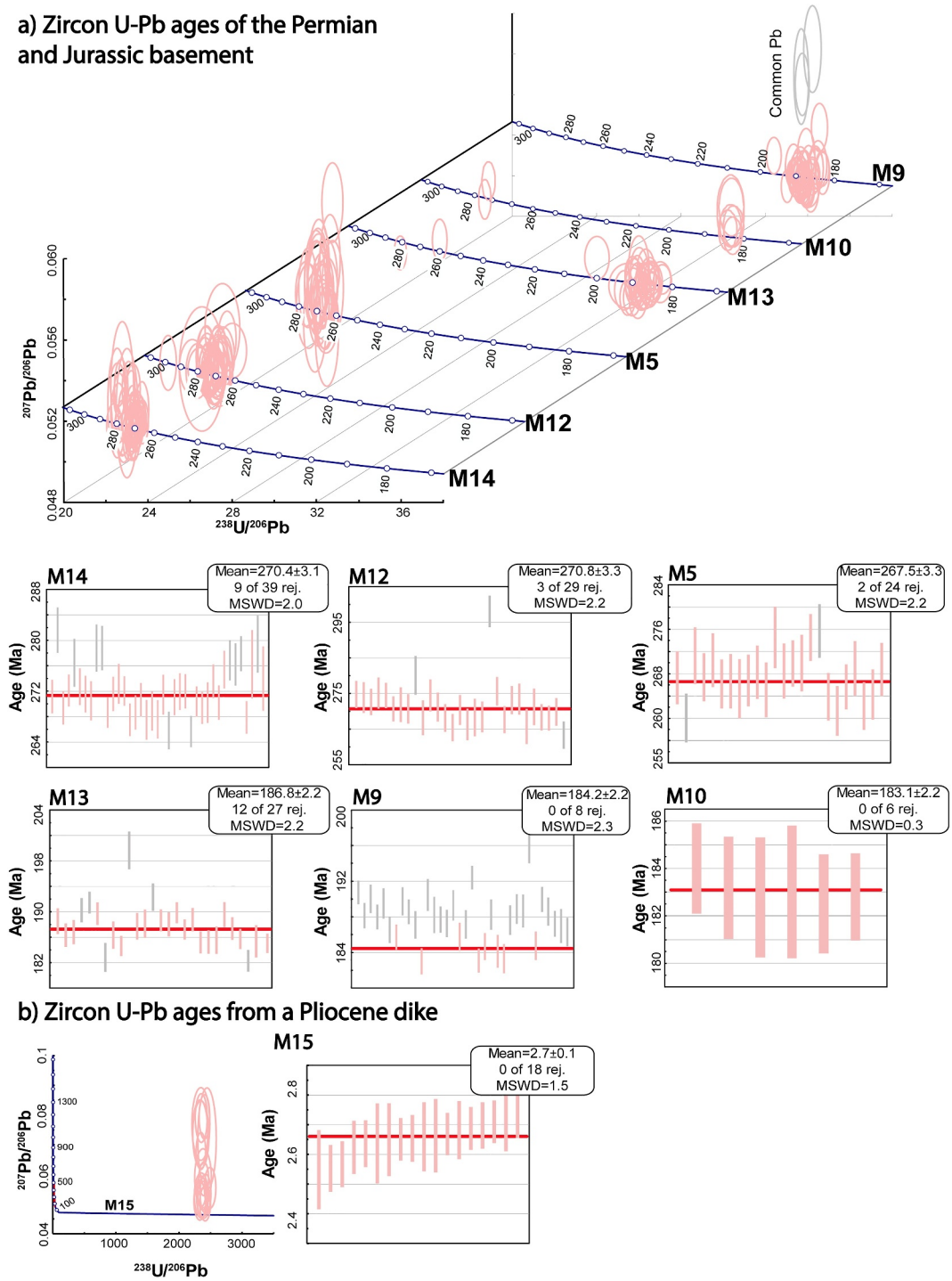

Figure 2. Zircon U-Pb ages, including Tera-Wasserburg Concordia and weighted average ^{238}U-^{206}Pb age calculations. Excluded grains are denoted in gray. Error bars at 2σ. Plotted using Isoplot 4.15 (Ludwig, 2007). (a) Permian to Jurassic zircon ages. (b) Zircon ages from a Pliocene dike.

respectively; Figure 1b). The PFS is an intra-basement structure oblique to the NNE Andean orogenic trend. In the studied area, the main fault trace of the CFS and the associated Frailes Fault cut the PFS, and place the Jurassic and Permian basement on top of the Cretaceous to Neogene sedimentary strata of the adjacent Upper Magdalena Basin. Within the core and damage zones of these two fault systems, a polyphase deformation history is evidenced

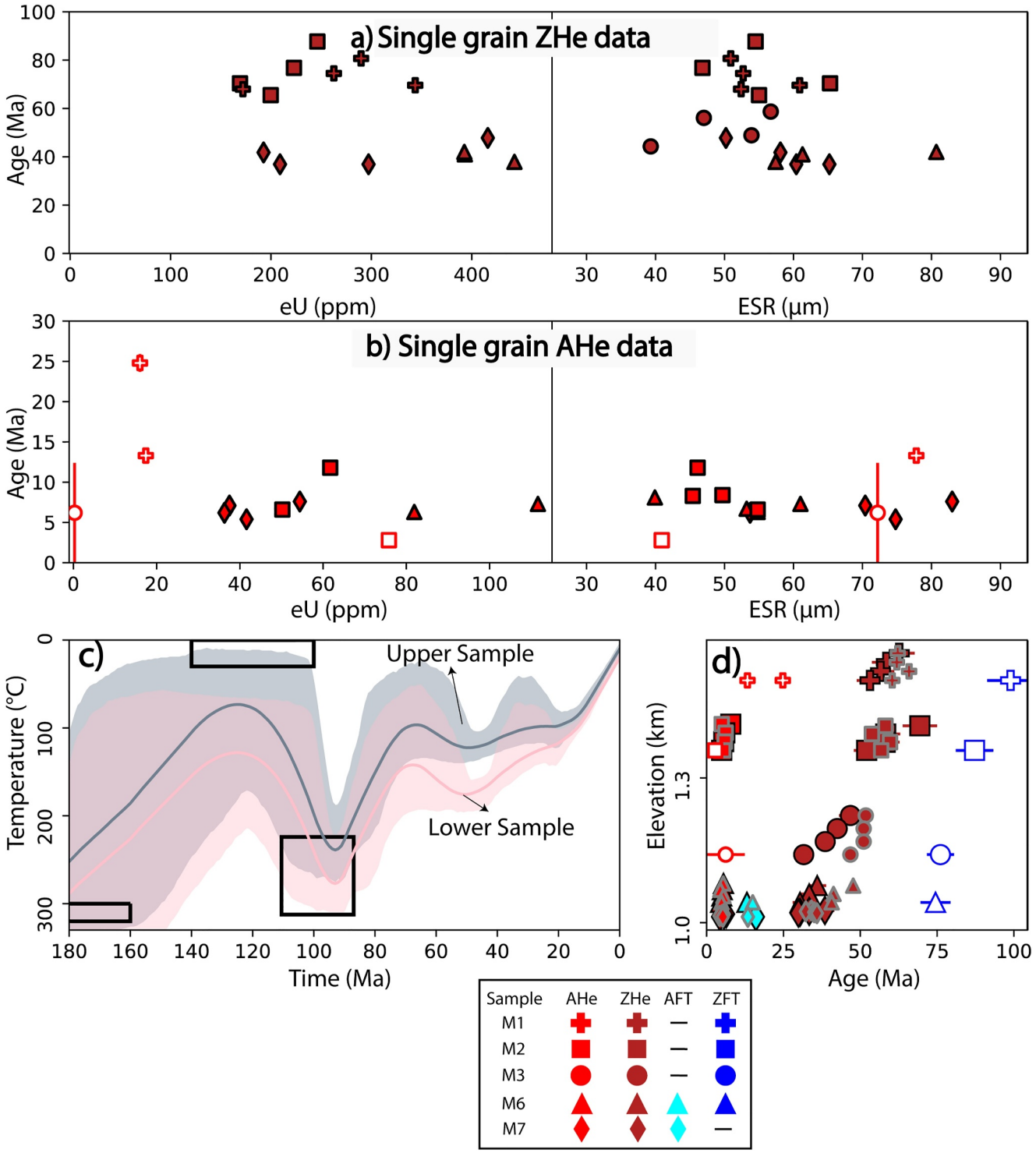

Figure 3. (a) and (b) Comparison of zircon (ZHe) and apatite (AHe) single grain (U-Th-Sm)/He ages against the Equivalent Spherical Radius (ESR) and the Effective Uranium (eU = U + 0.238*Th), a symbol with no fill indicates an excluded crystal. (c) Inverse thermal history model: gray and pink shading represent the 2-sigma confidence intervals for the expected models of the upper and lower samples; black boxes signify geological constraints. (d) Age versus elevation plot displaying both observed (symbols with black border) and predicted data (symbols with gray border). The crystals excluded from the model are presented with no symbol fill. Samples are differentiated by marker shape; while fill colors represent the thermochronological method.

10.1029/2024TC008340

Table 1
Sample Locations and Geo- and Thermo-Chronological Age

			Age ±2 sigma error (Ma)										
Sample	Longitude	Latitude	Zircon U-Pb	Apatite U-Pb	Titanite U-Pb	Epidote U-Pb	Illite K-Ar 2–6 μm	Illite K-Ar < 2 μm	Illite K-Ar < 0.2 μm	Zircon fission track	Zircon (U-Th)/He[a]	Apatite fission track	Apatite (U-Th-Sm)/He[a]
M1	−75.9779	2.6742								98.9 ± 7.6	75.6 ± 5.8		14.4 ± 0.9
M2	−75.9824	2.6216								87.2 ± 6.1	76.9 ± 9.7		9.0 ± 2.1
M3	−75.9661	2.5074								76.1 ± 4.4	52.8 ± 6.7		6.5 ± 6.5
M4	−75.9183	2.4642					58.6 ± 1.1	41.6 ± 1.2	37.3 ± 0.8				
M5	−75.9173	2.4642	267.5 ± 3.3		110.5 ± 1.6		171.2 ± 4.4	148.4 ± 4.6	99.1 ± 2.4				
M6	−75.9183	2.4642		181.0 ± 3.0						74.5 ± 4.9	40.3 ± 2.2	13.2 ± 0.8	7.1 ± 0.8
M7	−75.9103	2.4454		180.6 ± 3.2							41.5 ± 5.5	16.0 ± 1.4	6.7 ± 1.0
M8	−75.9179	2.4580				79.0 ± 5.8[b]							
						103.0 ± 18.0[c]							
M9	−75.9661	2.5074	184.2 ± 2.2										
M10	−75.9824	2.4047	183.1 ± 2.2										
M11	−75.8966	2.4130						66.4 ± 0.7	67.4 ± 1.8				
M12	−75.9301	2.4784	270.8 ± 3.3										
M13	−75.9195	2.4047	186.8 ± 2.2										
M14	−75.9804	2.2829	270.4 ± 3.1										
M15	−75.9804	2.2829	2.7 ± 0.1										

Note. Detailed data are provided in Tables S2–S5 in Supporting Information S1. [a]Mean ages from reproducible aliquots. [b]Disseminated epidote in matrix. [c]Vein-related epidote.

by the presence of mylonite zones, epidote and calcite veins, cataclastic breccia bands of titanite, muscovite and clay minerals, and fault gouges.

4.2. Zircon U-Pb Results From the Igneous Basement

U-Pb zircon ages were obtained from five plutonic rocks and two dikes associated with the Paez and the La Plata plutons (Figure 2). Two plutonic rocks (samples M14 and M12) and one mylonite (sample M5) from the La Plata Pluton exhibit similar Permian ages of 270.4 ± 3.1 Ma (n = 39; MSWD = 2.0), 270.8 ± 3.3 Ma (n = 29; MSWD = 2.2), and 267.5 ± 3.3 Ma (n = 24; MSWD = 2.2), respectively (Figure 2a). Zircons from these samples have length-width ratios (l:w) that vary from 2:1 to 3:1. Cathodoluminescence (CL) images from these zircons show that most of them have an oscillatory zoning pattern, typical of magmatic zircons (Corfu et al., 2003), some xenocrysts have patchy zoning, homogeneous cores, and complex growth rims. Two plutonic rocks, samples M13 and M9, from the Paez Pluton yielded Jurassic ages of 186.8 ± 2.2 Ma (n = 27; MSWD = 2.2) and 184.2 ± 2.2 (n = 8; MSWD = 2.3), respectively (Figure 2a).

Samples M10 and M15 correspond to two dikes characterized by zircons with l:w ratios varying from 1.5:1 to 3:1. Sample M10 that intruded the Jurassic pluton has zircon grains with an oscillatory zoned pattern with homogeneous cores surrounded by zoned rims. These grains yielded an age of 183.1 ± 2.2 Ma (n = 6, MSWD = 0.3, Figure 2a). Dike sample M15 that intruded the Permian pluton had zircons with oscillatory zoning patterns that yielded an age of 2.7 ± 0.1 Ma (n = 18; MSWD = 1.5) (Figure 2b).

4.3. Thermochronological Results

Five AHe, two AFT, five ZHe, and four ZFT dates were obtained from five samples collected along the hanging wall of the CFS and across the PFS (Figure 1). Sample elevations were between 1,000 and 1,600 m.a.s.l. Two AFT ages of 13.2 ± 0.8 and 16.0 ± 1.4 Ma were obtained for samples M6 and M7, respectively. ZFT ages range between 74.5 ± 4.9 and 98.9 ± 7.6 Ma, showing a positive relationship with elevation (Table S4 in Supporting Information S1, Figure 3d).

Sixteen single-grain AHe ages were obtained from samples M1, M2, M3, M7, and M6 (Table S5 in Supporting Information S1). Only one age of 6.2 ± 6.2 Ma was obtained from sample M3, while sample M1 yielded two ages of 13.3 ± 0.3 and 24.8 ± 1.0 Ma (Figure 3b); ages from these two samples were excluded due to the lack of intrasample reproducibility. Sample M2 has four reproducible ages between 6.6 ± 0.3 and 11.8 ± 0.3 Ma, and an age of 2.8 ± 0.2 Ma, which was considered an outlier. Sample M6 yielded four reproducible ages between 6.3 ± 0.3 and 8.1 ± 0.2 Ma. Finally, sample M7 yielded four reproducible ages between 5.4 ± 0.2 and 7.6 ± 0.2 Ma. Nineteen ZHe single grain ages were obtained from samples M1, M2, M3, M6, and M7. These samples exhibit good intrasample age reproducibility and a positive correlation between age and elevation (Figure 3a). The three lower samples (M7, M6, and M3) have similar single grain ages between 36.9 ± 0.5 Ma and 58.7 ± 0.8 Ma, while the two higher samples (M1 and M2) have ages between 65.5 ± 1.3 Ma and 87.7 ± 0.6 Ma (Figure 3a).

The expected inverse thermal history model indicates Jurassic cooling, followed by reheating in the Early Cretaceous and subsequent cooling during the Late Cretaceous. This model also suggests slow cooling throughout the Eocene-Oligocene, followed by a final Miocene cooling event (Figure 3c).

4.4. Structural Relations and Direct Dating of Fault-Related Neoformed Minerals

4.4.1. Field, Petrographic, and Geochronological Data From the Paez Fault System (PFS)

This fault system is characterized by a dominant high-angle NW-SE strike-slip geometry (mean plane N22°W/65°NE) with dextral and sinistral displacement components, as evidenced by the fault strikes (Figures 4a and 4b). Andesitic and doleritic dike swarms were observed intruding the Permian and Jurassic plutons and following a NW-strike, similar to the fractures and faults within the PFS damage zone (Figure 4b). In the PFS fault core, we identified a dominant NW-striking shear zone (mean plane of N47°W/68°NE) characterized by the presence of mylonite and gouge rocks, sample M5 was collected from the mylonite domain and sample M4 from the adjacent gouge.

10.1029/2024TC008340

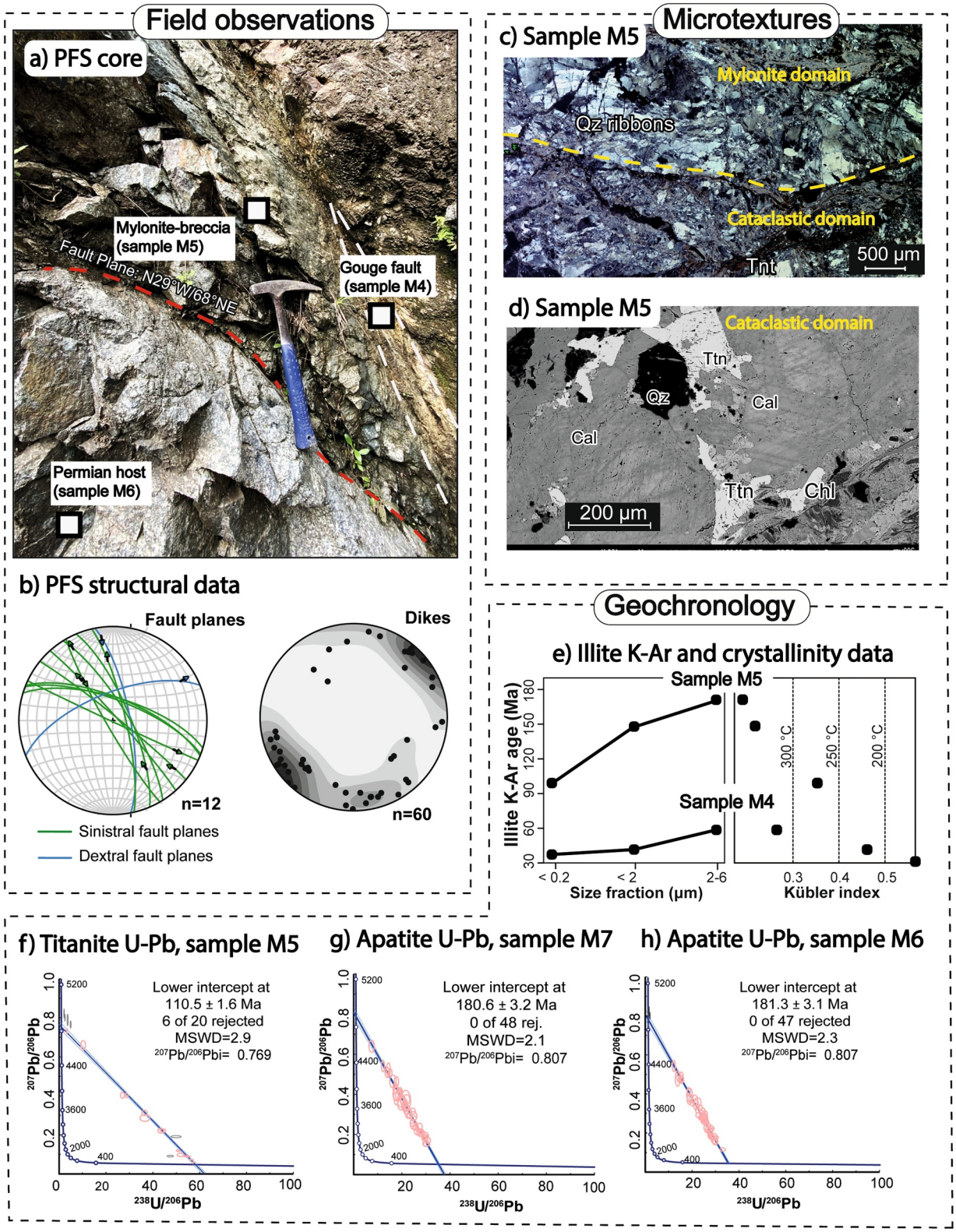

Figure 4.

4.4.1.1. Microstructural Analysis

The microstructural analysis of a mylonite rock (sample M5) in the core of the PFS reveals two main textural domains: (a) a predominant ductile mylonite and (b) a superimposed cataclastic breccia (Figure 4c), none of these domains present useful kinematic indicators.

The mylonite textural domain (a) exhibits a protomylonitic fabric characterized by an asymmetric foliation defined by elongate feldspars and boudinaged quartz ribbons (Figure 4c). Quartz microstructures include undulose extinction, subgrain rotation, and grain boundary migration recrystallization (Figure 4c). These features are evidence of solid-state deformation mechanisms at medium-temperature conditions ranging between 550 and 600°C, while in some areas, the bulging recrystallization of quartz suggests increasing shear strain with decreasing temperature (<500°C) (Passchier & Trouw, 2005; Stipp et al., 2002).

Domain (b) was formed by a micro-fracturing event that cuts across the quartz ribbons, resulting in the formation of cataclastic breccia and fluid circulation. This event led to significant alteration of the quartz-feldspathic protolith and widespread precipitation of Fe-oxides and clay-rich minerals (illite + smectite grains) in the breccia domains (Figure 4c). This textural domain displays a chaotic texture that includes highly fractured coarse-grained feldspars and quartz grains within a matrix composed of clay minerals and recrystallized fine-grained quartz. This domain is also characterized by the presence of micro-shear bands with several titanite grains as interstitial fillings among the neocrystallized calcite, muscovite, chlorite, and sericite grains (Figure 4c). Titanite grains are generally subhedral to anhedral, and their microstructures observed in backscattered electron images (BSE) show homogeneous bright domains and intragranular microcracks (Figure 4d).

4.4.1.2. Geochronology (Illite K-Ar, Titanite U-Pb, and Apatite U-Pb) and XRD Data of the PFS Fault Rocks

From the results of 47 apatite grains from the sample M6, we obtained a Tera-Wasserburg lower intercept U-Pb age of 181.3 ± 3.3 Ma with an MSWD = 2.3 (Figure 4h). Sample M7 exhibits 48 apatite grains with an intercept U-Pb age of 180.6 ± 3.2 Ma and an MSWD = 2.1 (Figure 4g). These ages contrast with the zircon U-Pb age from the adjacent samples M5 and M12 (267.5 ± 3.3 and 270.8 ± 3.3, described in chapter 4.1, which are directly related to the crystallization of the Permian La Plata Pluton.

Mylonite and cataclastic breccia textural domains were identified in sample M5. This sample yielded an inclined illite K-Ar age spectrum, with ages younger than the Permian host rock and the Jurassic intrusion. The coarser fractions (>0.2 μm) crystallized at 171 ± 4.4 Ma and 148.4 ± 4.6 Ma with IC values indicating epizone conditions (>300°C), while the finer fraction (<0.2 μm) yielded an age of 99.1 ± 2.4 Ma and formation temperatures within the upper anchizone (250–300°C) (Table S3 in Supporting Information S1 and Figure 4e). The crystallization conditions of the two coarser and older size fractions are consistent with the deformational temperatures inferred for the mylonite domain, while the younger and finer fractions show conditions consistent with the more brittle deformation in the cataclastic domains. Titanite U-Pb ages obtained for 14 grains from sample M5 yield an intercept age of 110.5 ± 1.6 Ma with an MSWD = 2.9 (Figure 4f). The Cretaceous titanite and illite ages confirm the microtextural observations, which suggest a similar origin for these minerals during the development of the cataclastic breccia domains.

Sample M4 was obtained from a clay-rich fault gouge within a ∼15 cm wide shear zone adjacent to the mylonite sample M5 (Figure 4a). The XRD profiles suggest the presence of neoformed minerals, such as, chlorite and illite ± smectite (Figure S1 in Supporting Information S1). This sample exhibits a bench-type age pattern with K-Ar illite ages between 37.3 ± 0.8 and 58 ± 1.1 Ma (Figure 4e). The two younger ages crystallized between the lower anchizone and diagenetic conditions (Table S2 in Supporting Information S1 and Figure 4e). The K-Ar illite ages obtained from the fault gouge differ from the crystallization ages of the host rock and the adjacent mylonite, suggesting multiple phases of illite formation and homogenization between ∼58 and 37 Ma (Hueck et al., 2022).

Figure 4. (a) Core of the Paez Fault System (PFS), showing the mylonite-breccia, fault gouge, and Permian monzogranite host. (b) Structural data from the PSF and associated dikes. (c) Microphotograph of mylonite and cataclastic domains in sample M5. (d) Subhedral to anhedral titanite crystals (highest back-scattered electron contrast) within the breccia domain in sample M5. (e) Illite K-Ar data and associated Kübler index from the mylonite (sample M5) and fault gouge (sample M4) in the core of the PSF. (f) Titanite U-Pb lower intercept age from the mylonite in the PFS core. (g)–(h) Apatite U-Pb ages from the Permian La Plata Pluton (sample M6) and the Jurassic Paez Pluton (sample M2).

4.4.2. Field, Petrological, and Geochronological Data From the Chusma Fault System (CFS)

The CFS has an NNE-SSW strike, the main fault plane in this fault System is N80°E/70NW and contains striae indicating dextral and sinistral strike-slip kinematics structure, some of which have reverse components (Figure 5c). The damage zone is characterized by high-angle unfilled fracture sets with NNE-SSW and NW-SE orientations. These structures are associated with a brittle deformation event that facilitated the generation of hydrothermal veins that crosscut the Jurassic pluton. These veins have a tabular geometry with lengths ranging between 10 and 30 cm and thicknesses between 3 and 6 cm, sample M8 was collected from one of these veins.

Along a fault core zone of the Chusma Fault System, sample M11 was collected from a gray fault gouge with an N55°E/42°SW orientation (Figure 5b). Notably, this gouge contains fragments of the quartz-monzodiorite host, which indicate fault frictional sliding deformation. Finally, inverse faults parallel to the trend of the CFS were observed displacing a dike with a zircon U-Pb age of 2.7 ± 0.1 Ma, as previously described in Section 4.1 (Figure 5d).

4.4.2.1. Microstructural Analysis and Epidote U-Pb Geochronology

The microstructural relationships between the fault veins and their host rock along the CFS were observed in the petrographic analyses of sample M8 (Figure 5e). This hydrothermal vein is composed of calcite-epidote ± quartz and shows sinuous contacts with the quartz-monzodiorite host. Calcite occurs as euhedral to subhedral crystals ranging between 500 and 1,000 μm, which fill the innermost part of the vein.

We distinguished two different types of epidote grains within the sample. Type 1 consists of medium- to coarse-grained (400–800 μm) euhedral to subhedral crystals, which co-precipitated with the calcite crystals and filled the outermost parts of the vein. Most of them show prismatic habits, patchy zoning, and several microcracks in BSE images (Figure 5f). Type 1 epidote grains returned a Tera–Wasserburg lower intercept age of 103.2 ± 18.0 Ma (MSWD = 2.4) with an initial $^{207}Pb/^{206}Pb$ ratio of 0.8373 ± 0.0027 (Figure 5i).

Epidotes grouped into textural type 2 are characterized by fine-grained anhedral crystals (<500 μm) disseminated throughout highly altered domains of the Jurassic quartz-monzodiorite host, indicating widespread hydrothermal fluid circulation within the sample (Figure 5e). BSE images show resorption zones in epidote grains (Putnis, 2009), microcracks, and ilmenite inclusions among these crystals (Figure 5g). For these grains, a Tera–Wasserburg lower intercept age of 79.0 ± 5.8 Ma with an MSWD of 2.4 and an initial $^{207}Pb/^{206}Pb$ ratio of 0.8093 ± 0.0057 was obtained from 19 data points (See details in Text S4 in Supporting Information S1, Figure 5j). The distinct initial $^{207}Pb/^{206}Pb$ ratios obtained for epidote types 1 and 2 confirm the textural observations, suggesting that these textural types were formed during different hydrothermal events.

4.4.2.2. Illite K-Ar Geochronology

The two finer fractions obtained from a gouge collected along the CFS (sample M11) yielded overlapping K-Ar ages around 67 Ma. This flat spectrum can be interpreted as a major event that homogenized the illite K-Ar system (Figure 5h). No useful IC data was obtained from this sample.

5. Tectonic and Deformation History of the NW South American Margin Recorded During the Structural Reworking of the Central Cordillera Basement

The Central Cordillera of the Colombian Andes can be considered a typical example of an orogenic system in which successive deformation phases reworked the preexisting basement. The structural evolution of the Central Cordillera has been mostly constrained by basement cooling (e.g., Restrepo-Moreno et al., 2009; Villagómez & Spikings, 2013; Zapata et al., 2021), and by the evolution of the sedimentary routing systems in the adjacent basins (e.g., Bayona, Baquero, et al., 2020; Horton et al., 2020; Pardo-Trujillo et al., 2020). As outlined below, this contribution reveals new phases and different styles of deformation in the southern Central Cordillera and their relations with major fault systems, improving the spatiotemporal resolution of the polyphase basement reworking in this mountain belt.

The tectono-structural evolution of the La Plata block in the southeastern segment of the Central Cordillera initiated at ~184 Ma, when mafic- to intermediate magmas associated with regional arc magmatism intruded the Permian La Plata Pluton at a depth of ~11 km (Siachoque et al., 2024). This magmatic event was associated with the intrusion of

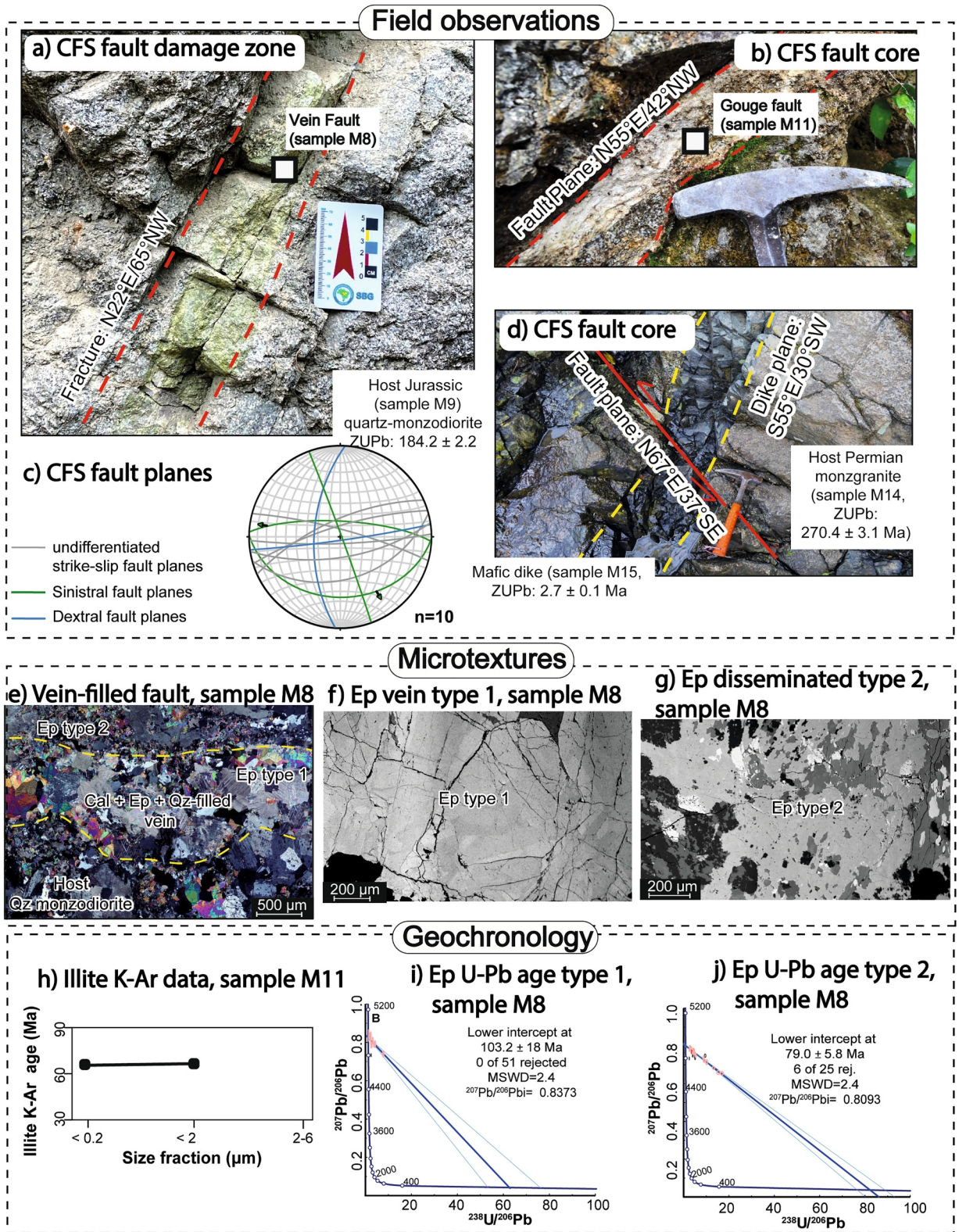

Figure 5. (a) Epidote alteration in fractures parallel to the CFS. (b) Fault gouge in the core of the Chusma Fault System (CFS). (c) Structural data from the CSF. (d) Deformed Pliocene mafic dikes in the core of the CFS. (e) Vein-fault showing two types of epidote grains. (f) Type 1 epidote crystals displaying patchy zoning textures and related microcracks. (g) Type 2 anhedral epidote crystal with corroded margins and several inclusions of Fe-Ti oxides. Mineral abbreviations according to Warr (2021). (h) K-Ar illite data from sample M11. (i) and (j) Tera-Wasserburg plots showing the epidote U-Pb ages from the two different textural groups.

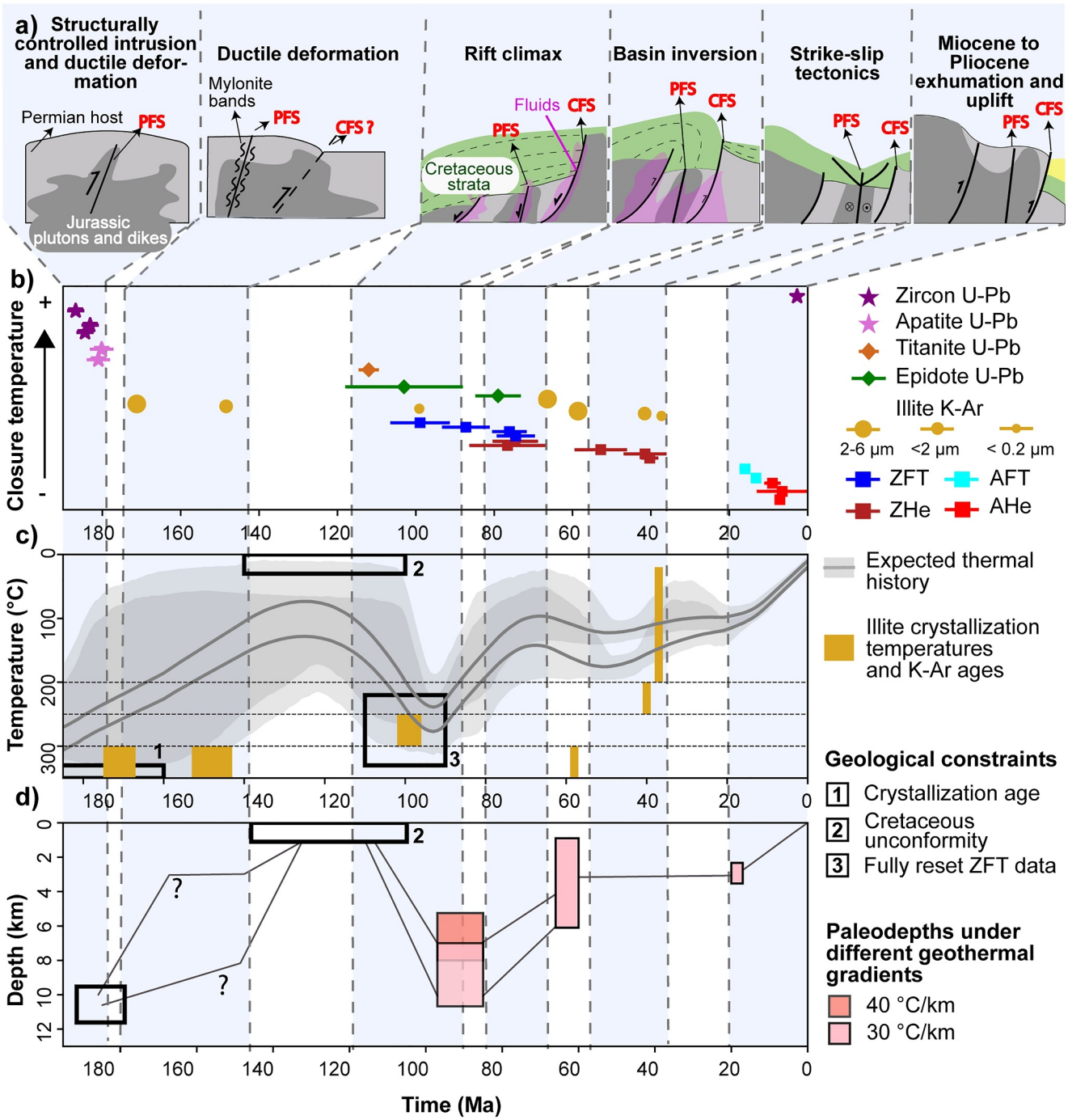

Figure 6. (a) Tectonic evolution of the Southern Central Cordillera, PFS: Paez Fault System, and CFS: Chusma Fault System. (b) Geo- and thermochronological data, symbol shapes and fill indicate the method. Permian zircon U-Pb ages are not presented. (c) Inverse thermal history model; black boxes denote geological constraints and the gold-filled boxes the age and temperature obtained for each illite size fraction. (d) Paleodepths derived from the thermal history model; colored boxes denote inferred paleodepths considering different geothermal gradients.

a dike swarm at ~183 Ma. These dikes have a dominant NW orientation parallel to the main strike of the PFS (Figure 4b), suggesting a structural control during their emplacement (Figure 6a), and implying a minimum Jurassic age for the development of this fault system. Apatite U-Pb from samples M6 and M7 within the Permian host yield overlapping ages at ~180 Ma. These ages are similar to the age of intrusion of the Paez Pluton magmas (Figure 6b), indicating temperature-driven resetting of the apatite U-Pb system in the Permian roof pendant.

The coarser illite fractions obtained from sample M5 in the core of the PFS suggest crystallization conditions exceeding 300°C and yield K-Ar ages of 171 ± 4.4 Ma and 148.4 ± 4.6 Ma; both ages are younger than the Permian protolith and the Early Jurassic event that reset the apatite U-Pb system. Given that the mylonite domains in sample M5 formed at temperatures between 450 and 600°C, the simplest interpretation is that these ages correspond to the recrystallization of illite during the brittle-ductile deformation of the Permian pluton. Additional evidence of Jurassic to Cretaceous deformation, includes the Lower Cretaceous strata on top of the Early Jurassic plutonic rocks, implying Middle Jurassic to Lower Cretaceous exhumation (Calderón-Díaz et al., 2023; Siachoque et al., 2024); and low- to middle-grade metamorphism in the western flank of the Central Cordillera (Blanco-Quintero et al., 2014).

The presence of Cretaceous strata on top of the Early Jurassic basement and ZHe and ZFT ages younger than sediment deposition imply Early Cretaceous reheating of the La Plata Block, which can be observed in the thermal history model (Figure 6c). This event is consistent with major rifting and sedimentation documented in the Upper and Middle Magdalena basins and the Northern Eastern and Central cordilleras between 140 and 100 Ma (Calderón-Díaz et al., 2023; Sarmiento & Rangel, 2004; Zapata et al., 2019). To reset the ZFT system (~232°C) under a relatively high geothermal gradient of 40°C/km and a surface temperature of 10°C, a minimum thickness of 5 km of Cretaceous sediments had to accumulate on top of the igneous basement (Figure 6d). This observation agrees with inferences farther north, which suggests that most of the Central Cordillera was a major sediment depocenter during the Early Cretaceous extensional phases (Cardona et al., 2019; Zapata et al., 2020).

This Early Cretaceous reheating event coincided with hydrothermal activity along both fault systems, as indicated by the overlapping titanite and epidote U-Pb ages at ~110 Ma (Figure 3). Within the PSF, hydrothermal activity was followed by the development of cataclastic bands at ~99 Ma, which overprinted the ductile Late Jurassic to Early Cretaceous mylonite fabric. Basement temperatures between 232 and 325°C can account for the brittle-ductile deformation textures, illite neoformation, and the resetting of ZHe and ZFT ages. Hydrothermal activity and the development of cataclastic bands between ~110 and 99 Ma provide an additional constraint on the extensional evolution of the Northern Andes, which has been reconstructed using sedimentary and magmatic patterns (Calderón-Díaz et al., 2023; Nie et al., 2010; Sarmiento-Rojas et al., 2006; Zapata et al., 2019). The documented Early Cretaceous evolution of the La Plata block exemplifies how reheating, brittle-ductile deformation, and hydrothermal activity modify the basement during syn-rift deformation (Figure 6a).

Basement cooling occurred between 100 and 65 Ma, as suggested by several of the ZFT and ZHe cooling ages. This event coincides with the U-Pb epidote crystallization age of ~79 Ma and the development of a fault gouge at ~67 Ma along the CFS (Figure 6b). Given that both epidote and illite ages independently indicate active deformation, exhumation and rock uplift were responsible for most of the cooling, rather than other processes such as post-rift cooling (Figure 6d). Exhumation between ~80 and 67 Ma can be temporally associated with the collision of the Caribbean Plateau, which was responsible for surface uplift and basin inversion in the north of the Central Cordillera and the Upper and Middle Magdalena basins between 72 and 62 Ma (Bayona et al., 2012; Calderon-Diaz et al., 2024; León et al., 2021; Vallejo et al., 2006; Zapata et al., 2021). Structurally controlled hydrothermal activity and fault gouge development in the La Plata Block provide direct evidence of basement deformation during the collision of the Caribbean Plateau in the Northern Andes.

The basement of the La Plata Block underwent slow cooling between ~55 and 30 Ma (Figure 6c). However, K-Ar dating of authigenic illite from a fault gouge along the PFS indicates active deformation between ~50 and 30 Ma (Figure 6b). Additionally, the kinematic indicators along the PFS suggest dominant strike-slip behavior associated with this event (Figure 4b), which is the last event documented for this fault system. Slow cooling rates, fault kinematic indicators, and fault gouge fabrics are direct evidence of Paleogene strike-slip deformation. This interpretation agrees with studies which have proposed that the Paleogene evolution of the Central Cordillera was characterized by dominant strike-slip tectonics and slow exhumation (Jaramillo et al., 2022; Lamus Ochoa et al., 2013; Villamizar-Escalante et al., 2021).

Assuming a post-rift geothermal gradient of 30°C/km, a surface temperature of 10°C, and a pre-exhumation temperature of 80°C (lower 2 sigma limit of the upper sample thermal history), our data implies that the La Plata Block underwent at least ~2.3 km of exhumation after ~20 Ma (Figure 6d). The offsetting of the ~2.7 Ma dikes by the CFS structures indicates that deformation persisted into the Pliocene. This Miocene to Pliocene exhumation event has also been documented in thermochronological data from farther north (Zapata et al., 2023), suggesting extended Miocene exhumation throughout the Southern Central Cordillera. Miocene to Pliocene rock

uplift and topographic growth have also been documented by seismic and provenance data from the Southern Central Cordillera and the Upper Magdalena Basin (Espitia et al., 2022; Ramon & Rosero, 2006).

6. Implications for Thick-Skinned Polyphase Orogens

Orogens dominated by thick-skinned tectonics are often characterized by multiple cycles of deformation responsible for the reworking and episodic exhumation of pre-orogenic crust, posing a challenge to unravel their deformation histories (Holdsworth et al., 1997; Pfiffner, 2017). Despite the multiple deformation events, the multi-chronometric approach presented here successfully provided direct insight into the polyphase evolution of the Central Cordillera, which can be used as a framework for understanding analogous orogenic processes.

Our results provide an example of differential and selective reactivation of the basement structures within discrete and continuous basement blocks. For instance, the NW-trending PFS is a pre-Andean structure older than the Jurassic magmatism and oblique to the continental margin. This structure-controlled magma emplacement during the Early Jurassic and the subsequent ductile deformation between ∼170 and 150 Ma. The mylonites or dike swarms described along the PFS were not observed in the CFS, suggesting a preferential reactivation of this structure. In contrast, hydrothermal activity and deformation during extension (∼110–99 Ma) and basin inversion (80–60 Ma) were documented along both fault systems, suggesting synchronous fault reactivation along the La Plata Block. In the Eocene-Oligocene, the PFS was selectively reactivated, experiencing strike-slip brittle deformation. A single thermal history was retrieved from thermochronological in the hanging wall of the CFS, suggesting that this structure may have been responsible for the vertical displacements of the basement during the Cretaceous and Miocene.

7. Conclusions

A multi-chronometric approach using nine geo- and thermochronological techniques reveal repeated basement reworking in the southern segment of the Central Cordillera of Colombia. The interpretation of the data shows that the Southern Central Cordillera basement experienced at least six deformational phases divided into four structural styles. (a) Pre-Andean compressional events, including structurally controlled Jurassic magmatism and Late Jurassic to Early Cretaceous ductile deformation. (b) Early Cretaceous extensional deformation characterized by hydrothermal activity, reheating, and brittle-ductile deformation. (c) Andean contractional deformation; basement cooling, percolation of fluids, and brittle deformation between ∼90 and 60 Ma characterized the onset of Andean deformation, while more recent Miocene and Pliocene Andean phases caused brittle deformation and exhumation. (d) Brittle Paleogene deformation and low basement exhumation rates linked to strike-slip tectonics. These styles exemplify the diverse array of tectonic settings and processes associated with fault reactivation.

This unique record of long-term fault reactivation documents the spatiotemporal relations between deformation-related processes such as plutonic and dike emplacement, hydrothermal activity, and rock mechanical modification, which together act as the major controls on the localization and nucleation of fault structures during deformation.

Data Availability Statement

All thermo- and geochronological data is available in the Geochron geodatabase (https://www.geochron.org/dataset/html/geochron_dataset_2024_07_29_PwVNU) (Zapata et al., 2024) and in the supplementary file.

Acknowledgments
The EGEO group acknowledges the funding from Minciencias and ANH through the agreement 785/668–2019 and the contract 80740-152-2021. D. Rubatto provided the reference materials for epidote U-Pb dating and F. Piccoli provided technical assistance during isotope measurements. The LA-ICP-MS facility at University of Bern, used for epidote U-Pb dating, was funded by the Swiss National Science Foundation, project 206021_170722 awarded to D. Rubatto and T. Pettke. David Chew acknowledges support from Science Foundation Ireland (SFI) through research Grant 13/RC/2092_P2 (iCRAG Research Centre).

References

Bakker, R. J., & Elburg, M. A. (2006). A magmatic-hydrothermal transition in Arkaroola (northern Flinders Ranges, South Australia): From diopside–titanite pegmatites to hematite–quartz growth. *Contributions to Mineralogy and Petrology*, *152*(5), 541–569. https://doi.org/10.1007/s00410-006-0125-0

Bayona, G. (2018). El inicio de la emergencia en los Andes del norte: Una perspectiva a partir del registro tectónico-sedimentológico del Coniaciano al Paleoceno. *Revista de la Academia Colombiana de Ciencias Exactas Fisicas y Naturales*, *42*(165), 364–378. https://doi.org/10.18257/raccefyn.632

Bayona, G., Baquero, M., Ramírez, C., Tabares, M., Salazar, A., Nova, G., et al. (2020). Unravelling the widening of the earliest Andean northern orogen: Maastrichtian to early Eocene intra-basinal deformation in the northern Eastern Cordillera of Colombia. *Basin Research*, *33*, 1–37. https://doi.org/10.1111/bre.12496

Bayona, G., Bustamante, C., Nova, G., Milena, A., & Franco, S. (2020). In J. Gómez & A. O. Pinilla–Pachon (Eds.), *Jurassic evolution of the northwestern corner of Gondwana: Present knowledge and future challenges in studying Colombian Jurassic rocks*. https://doi.org/10.32685/pub.esp.36.2019.05

Bayona, G., Cardona, A., Jaramillo, C., Mora, A., Montes, C., Caballero, V., et al. (2013). Onset of fault reactivation in the Eastern Cordillera of Colombia and proximal Llanos Basin; response to Caribbean–South American convergence in early Palaeogene time. *Geological Society, London, Special Publications*, *377*(1), 285–314. https://doi.org/10.1144/SP377.5

Bayona, G., Cardona, A., Jaramillo, C., Mora, A., Montes, C., Valencia, V., et al. (2012). Early Paleogene magmatism in the northern Andes: Insights on the effects of Oceanic Plateau–continent convergence. *Earth and Planetary Science Letters*, *331*, 97–111. https://doi.org/10.1016/j.epsl.2012.03.015

Bernet, M. (2009). A field-based estimate of the zircon fission-track closure temperature. *Chemical Geology*, *259*(3–4), 181–189. https://doi.org/10.1016/j.chemgeo.2008.10.043

Bird, D. K., & Spieler, A. R. (2004). Epidote in geothermal systems. *Reviews in Mineralogy and Geochemistry*, *56*(1), 235–300. https://doi.org/10.2138/gsrmg.56.1.235

Blanco-Quintero, I. F., García-Casco, A., Toro, L. M., Moreno, M., Ruiz, E. C., Vinasco, C. J., et al. (2014). Late Jurassic terrane collision in the northwestern margin of Gondwana (Cajamarca Complex, eastern flank of the Central Cordillera, Colombia). *International Geology Review*, *56*(15), 1852–1872. https://doi.org/10.1080/00206814.2014.963710

Brown, R. W., Beucher, R., Roper, S., Persano, C., Stuart, F., & Fitzgerald, P. (2013). Natural age dispersion arising from the analysis of broken crystals. Part I: Theoretical basis and implications for the apatite (U-Th)/He thermochronometer. *Geochimica et Cosmochimica Acta*, *122*, 478–497. https://doi.org/10.1016/j.gca.2013.05.041

Bustamante, C., Archanjo, C. J., Cardona, A., & Vervoort, J. D. (2016). Late Jurassic to Early Cretaceous plutonism in the Colombian Andes: A record of long-term arc maturity. *Geological Society of America Bulletin*, *128*(11–12), 1762–1779. https://doi.org/10.1130/b31307.1

Butler, R. W. H., Bond, C. E., Shipton, Z. K., Jones, R. R., & Casey, M. (2008). Fabric anisotropy controls faulting in the continental crust. *Journal of the Geological Society*, *165*(2), 449–452. https://doi.org/10.1144/0016-76492007-129

Calderon-Diaz, L., Zapata, S., Cardona, A., Parra, M., Sobel, E. R., Patiño, A. M., et al. (2024). Cretaceous extensional and contractional stages in the Colombian Andes unraveled by a source-to-sink geochronological and thermochronological study in the Upper Magdalena Basin. *Tectonophysics*, *878*, 230303. https://doi.org/10.1016/j.tecto.2024.230303

Calderón-Díaz, L. C., Zapata, S., Cardona, A., Parra, M., Sobel, E. R., Patiño, A. M., et al. (2023). Cretaceous extensional and compressional stages in the Colombian Andes unraveled by a source-to-sink geo- and thermochronogical study in the Upper Magdalena Basin. *SSRN*. https://doi.org/10.2139/ssrn.4591621

Cardona, A., León, S., Jaramillo, J. S., Valencia, V., Zapata, S., Pardo-Trujillo, A., et al. (2020). Cretaceous record from a Mariana to an Andeantype margin in the central cordillera of the Colombian Andes. In J. Gómez & A. O. Pinilla-Pachón (Eds.), *The Geology of Colombia* (Vol. 36, pp. 353–395).

Cardona, A., León, S., Jaramillo, J. S., Valencia, V., Zapata, S., Pardo–Trujillo, A., et al. (2019). Cretaceous record from a Mariana to an Andean–Type Margin in the Central Cordillera of the Colombian Andes. In J. Gómez & A. O. Pinilla–Pachon (Eds.), *The Geology of Colombia* (Vol. 2, pp. 353–395). Servicion Geologico Colombiano, Publicaciones Geológicas Especiales. https://doi.org/10.32685/pub.esp.36.2019.1

Carlson, W. D., Donelick, R. A., & Ketcham, R. A. (1999). Variability of apatite fission-track annealing kinetics: I. Experimental results. *American Mineralogist*, *84*(9), 1213–1223. https://doi.org/10.2138/am-1999-0901

Carvajal-Torres, J., Catuneanu, O., Mora, A., Caballero, V., & Reyes, M. (2022). First-order stratigraphic boundaries of the Late Cretaceous–Paleogene retroarc foreland basin in Colombia. *Frontiers in Earth Science*, *10*, 876140. https://doi.org/10.3389/feart.2022.876140

Ceccato, A., Behr, W. M., Zappone, A. S., Tavazzani, L., & Giuliani, A. (2024). Structural evolution, exhumation rates, and rheology of the European crust during Alpine collision: Constraints from the Rotondo granite—Gotthard nappe. *Tectonics*, *43*(6), e2023TC008219. https://doi.org/10.1029/2023tc008219

Chang, Z., Vervoort, J. D., McClelland, W. C., & Knaack, C. (2006). U-Pb dating of zircon by LA-ICP-MS. *Geochemistry, Geophysics, Geosystems*, *7*(5), 1–14. https://doi.org/10.1029/2005gc001100

Chew, D., Petrus, J. A., & Kamber, B. S. (2014). U–Pb LA–ICPMS dating using accessory mineral standards with variable common Pb. *Chemical Geology*, *363*, 185–199. https://doi.org/10.1016/j.chemgeo.2013.11.006

Chew, D., & Spikings, R. (2021). Apatite U-Pb thermochronology: A review. *Minerals*, *11*(10), 1095. https://doi.org/10.3390/min11101095

Corfu, F. (2013). A century of U-Pb geochronology: The long quest towards concordance. *Bulletin*, *125*(1–2), 33–47. https://doi.org/10.1130/b30698.1

Corfu, F., Hanchar, J. M., Hoskin, P. W. O., & Kinny, P. (2003). Atlas of zircon textures. *Reviews in Mineralogy and Geochemistry*, *53*, 469–500.

Costantino, D., Paton, D., & Mora, A. (2021). Structural style and kinematic history of the Colombian Eastern Cordillera. *Frontiers in Earth Science*, *9*, 1–25. https://doi.org/10.3389/feart.2021.636458

Dodson, M. H. (1973). Closure temperature in cooling geochronological and petrological systems. *Contributions to Mineralogy and Petrology*, *40*(3), 259–274. https://doi.org/10.1007/BF00373790

Ehlers, T. A., & Farley, K. A. (2003). Apatite (U-Th)/He thermochronometry: Methods and applications to problems in tectonic and surface processes. *Earth and Planetary Science Letters*, *206*(1–2), 1–14. https://doi.org/10.1016/S0012-821X(02)01069-5

Espitia, W., Cortés, M., Beltrán, W., Díaz, I. C. H., & Arias, J. (2022). Structural styles of the Upper Magdalena valley, Northern Andes, Colombia: Case studies. In *Andean Structural Styles* (pp. 139–148). Elsevier.

Farley, K. A. (2002). (U-Th)/He dating: Techniques, calibrations, and applications. *Reviews in Mineralogy and Geochemistry*, *47*(1), 819–844. https://doi.org/10.2138/rmg.2002.47.18

Fitz-Diaz, E., & van der Pluijm, B. (2013). Fold dating: A new Ar/Ar illite dating application to constrain the age of deformation in shallow crustal rocks. *Journal of Structural Geology*, *54*, 174–179. https://doi.org/10.1016/j.jsg.2013.05.011

Flowers, R. M. (2009). Exploiting radiation damage control on apatite (U–Th)/He dates in cratonic regions. *Earth and Planetary Science Letters*, *277*(1–2), 148–155. https://doi.org/10.1016/j.epsl.2008.10.005

Flowers, R. M., & Kelley, S. A. (2011). Interpreting data dispersion and " inverted " dates in apatite (U–Th)/He and fission-track datasets: An example from the US midcontinent. *Geochimical et Cosmochimica Acta*, *75*(18), 5169–5186. https://doi.org/10.1016/j.gca.2011.06.016

Flowers, R. M., Ketcham, R. A., Shuster, D. L., & Farley, K. A. (2009). Apatite (U–Th)/He thermochronometry using a radiation damage accumulation and annealing model. *Geochimica et Cosmochimica Acta*, *73*(8), 2347–2365. https://doi.org/10.1016/j.gca.2009.01.015

Frost, B. R., Chamberlain, K. R., & Schumacher, J. C. (2001). Sphene (titanite): Phase relations and role as a geochronometer. *Chemical Geology*, *172*(1–2), 131–148. https://doi.org/10.1016/s0009-2541(00)00240-0

Gallagher, K. (2012). Transdimensional inverse thermal history modeling for quantitative thermochronology. *Journal of Geophysical Research*, *117*(B2), 1–16. https://doi.org/10.1029/2011JB008825

Gallagher, K., Charvin, K., Nielsen, S., Sambridge, M., & Stephenson, J. (2009). Markov chain Monte Carlo (MCMC) sampling methods to determine optimal models, model resolution and model choice for Earth Science problems. *Marine and Petroleum Geology*, *26*(4), 525–535. https://doi.org/10.1016/j.marpetgeo.2009.01.003

Gehrels, G. E. (2012). Detrital zircon U-Pb geochronology: Current methods and new opportunities. *Recent advances in tectonics of sedimentary basins* (pp. 47–62).

Green, P. F., Duddy, I. R., Gleadow, A. J. W., Tingate, P. R., & Laslett, G. M. (1986). Thermal annealing of fission tracks in apatite: 1. A qualitative description. *Chemical Geology: Isotope Geoscience section*, *59*, 237–253. https://doi.org/10.1016/0168-9622(86)90074-6

Guenthner, W. R., Reiners, P. W., Ketcham, R. A., Nasdala, L., & Giester, G. (2013). Helium diffusion in natural zircon: Radiation damage, anisotropy, and the interpretation of zircon (U-Th)/He thermochronology. *American Journal of Science*, *313*(3), 145–198. https://doi.org/10.2475/03.2013.01

Harrison, T. M. (2005). Fundamentals of noble gas thermochronometry. *Reviews in Mineralogy and Geochemistry*, *58*(1), 123–149. https://doi.org/10.2138/rmg.2005.58.5

Hincapié-Gómez, S., Cardona, A., Jiménez, G., Monsalve, G., Ramírez-Hoyos, L., & Bayona, G. (2018). Paleomagnetic and gravimetrical reconnaissance of Cretaceous volcanic rocks from the Western Colombian Andes: Paleogeographic connections with the Caribbean Plate. *Studia Geophysica et Geodaetica*, *62*(3), 485–511. https://doi.org/10.1007/s11200-016-0678-y

Holdsworth, R. E., Butler, C. A., & Roberts, A. M. (1997). The recognition of reactivation during continental deformation. *Journal of the Geological Society*, *154*(1), 73–78. https://doi.org/10.1144/gsjgs.154.1.0073

Holdsworth, R. E., Hand, M., Miller, J. A., & Buick, I. S. (2001). Continental reactivation and reworking: An introduction. *Geological Society, London, Special Publications*, *184*(1), 1–12. https://doi.org/10.1144/gsl.sp.2001.184.01.01

Holdsworth, R. E., Stewart, M., Imber, J., & Strachan, R. A. (2001). The structure and rheological evolution of reactivated continental fault zones: A review and case study. *Geological Society, London, Special Publications*, *184*(1), 115–137. https://doi.org/10.1144/gsl.sp.2001.184.01.07

Horton, B. K., & Folguera, A. (2022). Tectonic inheritance and structural styles in the Andean fold-thrust belt and foreland basin. *Andean Structural Styles* (pp. 3–28). Elsevier.

Horton, B. K., Parra, M., & Mora Sr, A. (2020). Construction of the Eastern Cordillera of Colombia: Insights from the sedimentary record. In *The Geology of Colombia* (Vol. 37, p. 22). Servicio Geológico Colombiano, Publicaciones Geológicas Especiales.

Hueck, M., Wemmer, K., Basei, M. A. S., Philipp, R. P., Oriolo, S., Heidelbach, F., et al. (2020). Dating recurrent shear zone activity and the transition from ductile to brittle deformation: White mica geochronology applied to the Neoproterozoic Dom Feliciano Belt in South Brazil. *Journal of Structural Geology*, *141*, 104199. https://doi.org/10.1016/j.jsg.2020.104199

Hueck, M., Wemmer, K., Ksienzyk, A. K., Kuehn, R., & Vogel, N. (2022). Potential, premises, and pitfalls of interpreting illite argon dates-A case study from the German Variscides. *Earth-Science Reviews*, *232*, 104133. https://doi.org/10.1016/j.earscirev.2022.104133

Jaboyedoff, M., Bussy, F., Kübler, B., & Thelin, P. (2001). Illite "crystallinity" revisited. *Clays and Clay Minerals*, *49*(2), 156–167. https://doi.org/10.1346/ccmn.2001.0490205

Jaramillo, J. S., Zapata, S., Carvalho, M., Cardona, A., Jaramillo, C., Crowley, J. L., et al. (2022). Diverse magmatic evolutionary trends of the Northern Andes unraveled by Paleocene to early Eocene detrital zircon geochemistry. *Geochemistry, Geophysics, Geosystems*, *23*(9), e2021GC010113. https://doi.org/10.1029/2021gc010113

Kammer, A., & Bermúdez, A. P. (2013). Evidencias sedimentológicas y estructurales para un origen paleógeno de la Falla de Chusma, Valle Superior del Magdalena, borde occidental de la sub-cuenca de Neiva. *Geología Colombiana*, *38*, 43–64.

Kent, A. J. R., & Cooper, K. M. (2018). How well do zircons record the thermal evolution of magmatic systems? *Geology*, *46*(2), 111–114. https://doi.org/10.1130/g39690.1

Kerr, A. C., & Tarney, J. (2005). Tectonic evolution of the Caribbean and northwestern South America: The case for accretion of two Late Cretaceous oceanic plateaus. *Geology*, *33*(4), 269–272. https://doi.org/10.1130/G21109.1

Ketcham, R. (2019). Fission-track annealing: From geologic observations to thermal history modeling. *Fission-track thermochronology and its application to geology* (pp. 49–75).

Ketcham, R. A. (2005). Forward and inverse modeling of low-temperature thermochronometry data. *Reviews in Mineralogy and Geochemistry*, *58*(1), 275–314. https://doi.org/10.2138/rmg.2005.58.11

Ketcham, R. A., Carter, A., Donelick, R. A., Barbarand, J., & Hurford, A. J. (2007). Improved measurement of fission-track annealing in apatite using c-axis projection. *American Mineralogist*, *92*(5–6), 789–798. https://doi.org/10.2138/am.2007.2280

Kirkland, C. L., Yakymchuk, C., Szilas, K., Evans, N., Hollis, J., McDonald, B., & Gardiner, N. J. (2018). Apatite: A U-Pb thermochronometer or geochronometer? *Lithos*, *318*, 143–157. https://doi.org/10.1016/j.lithos.2018.08.007

Kralik, M., Krumm, H., & Schramm, J.-M. (1987). Low grade and very low grade metamorphism in the Northern Calcareous Alps and in the Greywacke Zone: Illite-crystallinity data and isotopic ages. In *Geodynamics of the Eastern Alps* (pp. 164–178). Deuticke.

Kübler, B., & Jaboyedoff, M. (2000). Illite crystallinity. *Comptes Rendus de l'Academie des Sciences - Series IIA: Earth and Planetary Science*, *331*(2), 75–89. https://doi.org/10.1016/s1251-8050(00)01395-1

Lamus Ochoa, F., Bayona, G., Cardona, A., & Mora, A. (2013). Provenance of Cenozoic units of the Guaduas syncline: Implication in the tectonic evolution of the south of middle Magdalena valley and adjacent orogens. *Boletin de Geologia*, *35*, 17–42.

Lee, J. K. W., Williams, I. S., & Ellis, D. J. (1997). Pb, U and Th diffusion in natural zircon. *Nature*, *390*(6656), 159–162. https://doi.org/10.1038/36554

León, S., Monsalve, G., & Bustamante, C. (2021). How much did the Colombian Andes rise by the collision of the Caribbean oceanic plateau? *Geophysical Research Letters*, *48*(7), e2021GL093362. https://doi.org/10.1029/2021gl093362

Ludwig, K. C. (2007). *User´s Manual for Isoplot 3.7*. Berkley Geochronology Center.

Montes, C., Rodriguez-Corcho, A. F., Bayona, G., Hoyos, N., Zapata, S., & Cardona, A. (2019). Continental margin response to multiple arc-continent collisions: The northern Andes-Caribbean margin. *Earth-Science Reviews*, *198*, 102903. https://doi.org/10.1016/j.earscirev.2019.102903

Mora, A., Parra, M., Strecker, M. R., Kammer, A., Dimaté, C., & Rodríguez, F. (2006). Cenozoic contractional reactivation of Mesozoic extensional structures in the Eastern Cordillera of Colombia. *Tectonics*, *25*(2), 1–19. https://doi.org/10.1029/2005TC001854

Mora, A., Villagómez, D., Parra, M., Caballero, V. M., Spikings, R., Horton, B., et al. (2020). Late Cretaceous to Cenozoic uplift of the northern Andes: Paleogeographic implications. *The Geology of Colombia*, *3*, 89–121.

Mora-Rojas, L., Cárdenas, A., Jaramillo, C., Silvestro, D., Bayona, G., Zapata, S., et al. (2023). Stratigraphy of a middle Miocene neotropical Lagerstätte (La Venta Site, Colombia). *Geodiversitas*, *45*(6), 197–221. https://doi.org/10.5252/geodiversitas2023v45a6

Moser, A. C., Hacker, B. R., Gehrels, G. E., Seward, G. G. E., Kylander-Clark, A. R. C., & Garber, J. M. (2022). Linking titanite U–Pb dates to coupled deformation and dissolution–reprecipitation. *Contributions to Mineralogy and Petrology*, *177*(3), 42. https://doi.org/10.1007/s00410-022-01906-9

Mottram, C. M., Kellett, D. A., Barresi, T., Zwingmann, H., Friend, M., Todd, A., & Percival, J. B. (2020). Syncing fault rock clocks: Direct comparison of U-Pb carbonate and K-Ar illite fault dating methods. *Geology*, *48*(12), 1179–1183. https://doi.org/10.1130/g47778.1

Nie, J., Horton, B. K., Mora, A., Saylor, J. E., Housh, T. B., Rubiano, J., & Naranjo, J. (2010). Tracking exhumation of Andean ranges bounding the Middle Magdalena Valley Basin, Colombia. *Geology*, *38*(5), 451–454. https://doi.org/10.1130/G30775.1

Nivia, A., Marriner, G. F., Kerr, A. C., & Tarney, J. (2006). The Quebrada Grande Complex: A Lower Cretaceous ensialic marginal basin in the Central Cordillera of the Colombian Andes. *Journal of South American Earth Sciences*, *21*(4), 423–436. https://doi.org/10.1016/j.jsames.2006.07.002

Noriega Londoño, S. (2016). *Geomorfología tectónica del noroccidente de la Cordillera Central, Andes del Norte - Colombia* (p. 151). Repositorio Universidad Nacional.

Noriega-Londoño, S., Restrepo-Moreno, S. A. A., Vinasco, C., Bermúdez, M. A. A., & Min, K. (2020). Thermochronologic and geomorphometric constraints on the Cenozoic landscape evolution of the Northern Andes: Northwestern Central Cordillera, Colombia. *Geomorphology*, *351*, 106890. https://doi.org/10.1016/j.geomorph.2019.106890

Nuriel, P., Craddock, J., Kylander-Clark, A. R. C., Uysal, I. T., Karabacak, V., Dirik, R. K., et al. (2019). Reactivation history of the North Anatolian fault zone based on calcite age-strain analyses. *Geology*, *47*(5), 465–469. https://doi.org/10.1130/g45727.1

Ott, R. F., Pérez-Consuegra, N., Scherler, D., Mora, A., Huppert, K. L., Braun, J., et al. (2023). Erosion rate maps highlight spatio-temporal patterns of uplift and quantify sediment export of the Northern Andes. *Earth and Planetary Science Letters*, *621*, 118354. https://doi.org/10.1016/j.epsl.2023.118354

Pardo-Trujillo, A., Cardona, A., Giraldo, A. S., León, S., Vallejo, D. F., Trejos-Tamayo, R., et al. (2020). Sedimentary record of the Cretaceous–Paleocene arc–continent collision in the northwestern Colombian Andes: Insights from stratigraphic and provenance constraints. *Sedimentary Geology*, *401*, 105627. https://doi.org/10.1016/j.sedgeo.2020.105627

Passchier, C. W., & Trouw, R. A. J. (2005). *Microtectonics*. Springer Science & Business Media.

Pearson, D. M., Kapp, P., DeCelles, P. G., Reiners, P. W., Gehrels, G. E. E., Ducea, M. N., & Pullen, A. (2013). Influence of pre-Andean crustal structure on Cenozoic thrust belt kinematics and shortening magnitude: Northwestern Argentina. *Geosphere*, *9*(6), 1766–1782. https://doi.org/10.1130/GES00923.1

Pérez-Consuegra, N., Hoke, G. D., Fitzgerald, P., Mora, A., Sobel, E. R., & Glodny, J. (2022). Late Miocene– Pliocene onset of fluvial incision of the Cauca River Canyon in the Northern Andes. *GSA Bulletin*, *134*(9–10), 2453–2468. https://doi.org/10.1130/b36047.1

Pérez-Consuegra, N., Ott, R. F., Hoke, G. D., Galve, J. P., Pérez-Peña, V., & Mora, A. (2021). Neogene variations in slab geometry drive topographic change and drainage reorganization in the Northern Andes of Colombia. *Global and Planetary Change*, *206*, 103641. https://doi.org/10.1016/j.gloplacha.2021.103641

Peverelli, V., Berger, A., Mulch, A., Pettke, T., Piccoli, F., & Herwegh, M. (2022). Epidote U-Pb geochronology and H isotope geochemistry trace pre-orogenic hydration of midcrustal granitoids. *Geology*, *50*(9), 1073–1077. https://doi.org/10.1130/g50028.1

Peverelli, V., Berger, A., Wille, M., Mulch, A., Lanari, P., Pettke, T., et al. (2023). Unravelling the hydration history of an inverted passive continental margin using epidote UPb geochronology and Pb–Sr–O–H isotope geochemistry. *Lithos*, *460*, 107391. https://doi.org/10.1016/j.lithos.2023.107391

Peverelli, V., Berger, A., Wille, M., Pettke, T., Lanari, P., Villa, I. M., & Herwegh, M. (2022). Epidote dissolution–precipitation during viscous granular flow: A micro-chemical and isotope study. *Solid Earth*, *13*(11), 1803–1821. https://doi.org/10.5194/se-13-1803-2022

Peverelli, V., Ewing, T., Rubatto, D., Wille, M., Berger, A., Villa, I. M., et al. (2021). U– Pb geochronology of epidote by laser ablation inductively coupled plasma mass spectrometry (LA-ICP-MS) as a tool for dating hydrothermal-vein formation. *Geochronology*, *3*(1), 123–147. https://doi.org/10.5194/gchron-3-123-2021

Pfiffner, O. A. (2017). Thick-skinned and thin-skinned tectonics: A global perspective. *Geosciences*, *7*(3), 71. https://doi.org/10.3390/geosciences7030071

Putnis, A. (2009). Mineral replacement reactions. *Reviews in Mineralogy and Geochemistry*, *70*(1), 87–124. https://doi.org/10.2138/rmg.2009.70.3

Ramon, J. C., & Rosero, A. (2006). Multiphase structural evolution of the western margin of the Girardot subbasin, Upper Magdalena Valley, Colombia. *Journal of South American Earth Sciences*, *21*(4), 493–509. https://doi.org/10.1016/j.jsames.2006.07.012

Reiners, P. W., & Brandon, M. T. (2006). Using thermochronology to understand orogenic erosion. *Annual Review of Earth and Planetary Sciences*, *34*(1), 419–466. https://doi.org/10.1146/annurev.earth.34.031405.125202

Reiners, P. W., & Zeitler, P. (2005). Past, present, and future of thermochronology. *Reviews in Mineralogy and Geochemistry*, *58*, 1–18. https://doi.org/10.2138/rmg.2005.58.1

Restrepo-Moreno, S. A., Foster, D. A., Bernet, M., Min, K., & Noriega, S. (2019). Morphotectonic and orogenic development of the northern Andes of Colombia: A low-temperature thermochronology perspective. *Frontiers in Earth Sciences*, 749–832. https://doi.org/10.1007/978-3-319-76132-9_11

Restrepo-Moreno, S. A., Foster, D. A., Stockli, D. F., & Parra-Sánchez, L. N. (2009). Long-term erosion and exhumation of the "Altiplano Antioqueño", Northern Andes (Colombia) from apatite (U–Th)/He thermochronology. *Earth and Planetary Science Letters*, *278*(1–2), 1–12. https://doi.org/10.1016/j.epsl.2008.09.037

Reyes-Harker, A., Ruiz-Valdivieso, C. F., Mora, A., Ramírez-Arias, J. C., Rodriguez, G., De La Parra, F., et al. (2015). Cenozoic paleogeography of the Andean foreland and retroarc hinterland of Colombia. *AAPG Bulletin*, *99*(08), 1407–1453. https://doi.org/10.1306/06181411110

Rodríguez-Cuevas, M., Cardona, A., Monsalve, G., Zapata, S., & Valencia-Gómez, J. C. (2024). Fracture evaluation of the plutonic basement in the Upper Magdalena Basin: Implications for the development of naturally fractured reservoirs in the Northern Andes. *Geological Journal*, *59*(7), 1968–1997. https://doi.org/10.1002/gj.4980

Rodríguez–García, G., Correa–Martínez, A. M., Zapata–Villada, J. P., & Obando–Erazo, G. (2019). Fragments of a Permian arc on the western margin of the Neoproterozoic basement of Colombia. *The Geology of Colombia*, *1*.

Sarmiento, L. F., & Rangel, A. (2004). Petroleum systems of the upper Magdalena Valley, Colombia. *Marine and Petroleum Geology*, *21*(3), 373–391. https://doi.org/10.1016/j.marpetgeo.2003.11.019

Sarmiento-Rojas, L. F., Van Wess, J. D., & Cloetingh, S. (2006). Mesozoic transtensional basin history of the Eastern Cordillera, Colombian Andes: Inferences from tectonic models. *Journal of South American Earth Sciences*, *21*(4), 383–411. https://doi.org/10.1016/j.jsames.2006.07.003

Schmidt, M. W., & Poli, S. (2004). Magmatic epidote. *Reviews in Mineralogy and Geochemistry*, *56*(1), 399–430. https://doi.org/10.2138/gsrmg.56.1.399

Schmitz, M. D., & Bowring, S. A. (2001). U-Pb zircon and titanite systematics of the Fish Canyon Tuff: An assessment of high-precision U-Pb geochronology and its application to young volcanic rocks. *Geochimica et Cosmochimica Acta*, *65*(15), 2571–2587. https://doi.org/10.1016/s0016-7037(01)00616-0

Siachoque, A., García-Chinchilla, D. A., Zapata, S., Cardona, A., Vlach, S. R. F., Bustamante, C., & Chavarría, L. F. (2024). Mineral chemistry and thermobarometry of Jurassic arc granitoids: Implications for petrotectonic and unroofing history of the southern Colombian Andes. *Geological Magazine*, 1–20. https://doi.org/10.1017/s0016756824000256

Spikings, R., Cochrane, R., Villagomez, D., Lelij, R. V. D., Vallejo, C., Winkler, W., et al. (2015). The geological history of northwestern South America: From Pangaea to the early collision of the Caribbean Large Igneous Province (290–75 Ma). *Gondwana Research*, *27*(1), 95–139. https://doi.org/10.1016/j.gr.2014.06.004

Spikings, R., & Simpson, G. (2014). Rock uplift and exhumation of continental margins by the collision, accretion, and subduction of buoyant and topographically prominent oceanic crust. *Tectonics*, *33*(5), 635–655. https://doi.org/10.1002/2013tc003425

Stewart, M., Holdsworth, R. E., & Strachan, R. A. (2000). Deformation processes and weakening mechanisms within the frictional–viscous transition zone of major crustal-scale faults: Insights from the Great Glen Fault Zone, Scotland. *Journal of Structural Geology*, *22*(5), 543–560. https://doi.org/10.1016/s0191-8141(99)00164-9

Stipp, M., Stünitz, H., Heilbronner, R., & Schmid, S. M. (2002). Dynamic recrystallization of quartz: Correlation between natural and experimental conditions. *Geological Society, London, Special Publications*, *200*(1), 171–190. https://doi.org/10.1144/gsl.sp.2001.200.01.11

Sun, J., Yang, J., Wu, F., Xie, L., Yang, Y., Liu, Z., & Li, X. (2012). In situ U-Pb dating of titanite by LA-ICPMS. *Chinese Science Bulletin*, *57*(20), 2506–2516. https://doi.org/10.1007/s11434-012-5177-0

Tsukamoto, S., Tagami, T., & Zwingmann, H. (2020). Direct dating of fault movement. In *Understanding faults* (pp. 257–282). Elsevier.

Valencia-Gómez, J. C., Cardona, A., Zapata, S., Monsalve, G., Marín, D., Rodríguez-Cuevas, M., et al. (2024). Fracture analysis and low-temperature thermochronology of faulted Jurassic igneous rocks in the Southern Colombian Andes: Reservoir and tectonic implications. *Marine and Petroleum Geology*, *165*, 106850. https://doi.org/10.1016/j.marpetgeo.2024.106850

Vallejo, C., Spikings, R., Winkler, W., Luxieux, L., Chew, D., & Page, L. (2006). The early interaction between the Caribbean Plateau and the NW South American plate. *Terra Nova*, *18*(4), 264–269. https://doi.org/10.1111/j.1365-3121.2006.00688.x

Villagómez, D., & Spikings, R. (2013). Thermochronology and tectonics of the Central and Western Cordilleras of Colombia: Early Cretaceous–Tertiary evolution of the Northern Andes. *Lithos*, *160–161*, 228–249. https://doi.org/10.1016/j.lithos.2012.12.008

Villamizar-Escalante, N., Bernet, M., Urueña-Suárez, C., Hernández-González, J. S., Terraza-Melo, R., Roncancio, J., et al. (2021). Thermal history of the southern Central Cordillera and its exhumation record in the Cenozoic deposits of the Upper Magdalena Valley, Colombia. *Journal of South American Earth Sciences*, *107*, 103105. https://doi.org/10.1016/j.jsames.2020.103105

Vinasco, C., & Cordani, U. (2012). Reactivation episodes of the Romeral Fault System in the northwestern part of Central Andes, Colombia, through ^{39}Ar-^{40}Ar and K-Ar results. *Boletín Ciencias de la Tierra*, *32*, 111–124.

Wagner, G. A., Gleadow, A. J. W. W., & Fitzgerald, P. G. (1989). The significance of the partial annealing zone in apatite fission-track analysis: Projected track length measurements and uplift chronology of the transantarctic mountains. *Chemical Geology: Isotope Geoscience Section*, *79*(4), 295–305. https://doi.org/10.1016/0168-9622(89)90035-3

Warr, L. N. (2021). IMA–CNMNC approved mineral symbols. *Mineralogical Magazine*, *85*, 291–320. https://doi.org/10.1180/mgm.2021.43

Zapata, S., Calderon-Diaz, L., Jaramillo, C., Oboh-Ikuenobe, F., Piedrahita, J. C., Rodríguez-Cuevas, M., et al. (2023). Drainage and sedimentary response of the Northern Andes and the Pebas system to Miocene strike-slip tectonics: A source to sink study of the Magdalena Basin. *Basin Research*, *35*(5), 1674–1717. https://doi.org/10.1111/bre.12769

Zapata, S., Cardona, A., Jaramillo, J. S., Patiño, A., Valencia, V., León, S., et al. (2019). Cretaceous extensional and compressional tectonics in the Northwestern Andes, prior to the collision with the Caribbean oceanic plateau. *Gondwana Research*, *66*, 207–226. https://doi.org/10.1016/j.gr.2018.10.008

Zapata, S., Cardona, A., Jaramillo-Rios, J. S., Siachoque, A., Peverelli, V., Chew, D., et al. (2024). Thermo- and Geochronological data from the Southern Central Cordillera in Colombia (Version 1) [Dataset]. *Geochron*. Retrieved from https://www.geochron.org/dataset/html/geochron_dataset_2024_07_29_PwVNU

Zapata, S., Patiño, A., Cardona, A., Parra, M., Valencia, V., Reiners, P., et al. (2020). Bedrock and detrital zircon thermochronology to unravel exhumation histories of accreted tectonic blocks: An example from the Western Colombian Andes. *Journal of South American Earth Sciences*, *103*, 102715. https://doi.org/10.1016/j.jsames.2020.102715

Zapata, S., Zapata-Henao, M., Cardona, A., Jaramillo, C., Silvestro, D., & Oboh-Ikuenobe, F. (2021). Long-term topographic growth and decay constrained by 3D thermo-kinematic modeling: Tectonic evolution of the Antioquia Altiplano, Northern Andes. *Global and Planetary Change*, *203*, 103553. https://doi.org/10.1016/j.gloplacha.2021.103553

References From the Supporting Information

Barth, H., Ganz, M., & Brandt, R. (1994). Upper concentration limits for 239Pu traces in some "KTB"-samples and in one Hawaiian lava. *Geochimica et Cosmochimica Acta*, *58*(21), 4759–4765. https://doi.org/10.1016/0016-7037(94)90206-2

Burn, M., Lanari, P., Pettke, T., & Engi, M. (2017). Non-matrix-matched standardisation in LA-ICP-MS analysis: General approach, and application to allanite Th–U–Pb dating. *Journal of Analytical Atomic Spectrometry*, *32*(7), 1359–1377. https://doi.org/10.1039/c7ja00095b

Chang, Z., Vervoort, J. D., McClelland, W. C., & C, K. (2006). U-Pb dating of zircon by LA-ICP-MS. *Geochemistry, Geophysics, Geosystems*, *7*(5), 1–14. https://doi.org/10.1029/2005gc001100

Chew, D. M., Petrus, J. A., & Kamber, B. S. (2014). U–Pb LA–ICPMS dating using accessory mineral standards with variable common Pb. *Chemical Geology*, *363*, 185–199. https://doi.org/10.1016/j.chemgeo.2013.11.006

Dumitru, T. (1993). FT STAge Systems, described. *Nuclear Tracks and Radiation Measurements*, *21*(4), 575–580. https://doi.org/10.1016/1359-0189(93)90198-i

Dunkl, I. (2002). Trackkey: A windows program for calculation and graphical presentation of fission track data. *Computers & Geosciences*, *28*(1), 3–12. https://doi.org/10.1016/S0098-3004(01)00024-3

Farley, K. A., Wolf, R. A., & Silver, L. T. (1996). The effects of long alpha-stopping distances on (U-Th)/He ages. *Geochimica et Cosmochimica Acta*, *60*(21), 4223–4229. https://doi.org/10.1016/s0016-7037(96)00193-7

Fisher, C. M., Bauer, A. M., Luo, Y., Sarkar, C., Hanchar, J. M., Vervoort, J. D., et al. (2020). Laser ablation split-stream analysis of the Sm-Nd and U-Pb isotope compositions of monazite, titanite, and apatite–Improvements, potential reference materials, and application to the Archean Saglek Block gneisses. *Chemical Geology*, *539*, 119493. https://doi.org/10.1016/j.chemgeo.2020.119493

Galbraith, R. F., & Laslett, G. M. (1993). Statistical models for mixed fission track ages. *Nuclear Tracks and Radiation Measurements*, *21*(4), 459–470. https://doi.org/10.1016/1359-0189(93)90185-c

Green, P. F. (1981). A new look at statistics in fission-track dating. *Nuclear Tracks*, *5*(1–2), 77–86. https://doi.org/10.1016/0191-278X(81)90029-9

Gregory, C. J., Rubatto, D., Allen, C. M., Williams, I. S., Hermann, J., & Ireland, T. (2007). Allanite micro-geochronology: A LA-ICP-MS and SHRIMP U–Th–Pb study. *Chemical Geology*, *245*(3–4), 162–182. https://doi.org/10.1016/j.chemgeo.2007.07.029

Hurford, A. J. (1998). Zeta: The ultimate solution to fission-track analysis calibration or just an interim measure? In *Advances in fission-track geochronology* (pp. 19–32). Springer.

Ketcham, R. A., Gautheron, C., & Tassan-Got, L. (2011). Accounting for long alpha-particle stopping distances in (U–Th–Sm)/He geochronology: Refinement of the baseline case. *Geochimica et Cosmochimica Acta*, *75*(24), 7779–7791. https://doi.org/10.1016/j.gca.2011.10.011

Kisch, H. J. (1991). Illite crystallinity: Recommendations on sample preparation, X-ray diffraction settings, and interlaboratory samples. *Journal of Metamorphic Geology*, *9*(6), 665–670. https://doi.org/10.1111/j.1525-1314.1991.tb00556.x

Kralik, M., Klima, K., & Riedmüller, G. (1987). Dating fault gouges. *Nature*, *327*(6120), 315–317. https://doi.org/10.1038/327315a0

Krumm, S. (1992). *Illitkristallinität als Indikator schwacher Metamorphose: methodische Untersuchungen, regionale Anwendungen und Vergleiche mit anderen Parametern*. Institut für Angewandte Geologie.

Kübler, B. (1967). La cristallinite de I'illite et les zones tout a fait superieures de metamorphisme. In *Etages Tectoniques, Colloque de Neuchâtel 1966* (pp. 105–121). A la Baconniere.

Kübler, B. (1984). Les indicateurs des transformations physiques et chimiques dans la diagenese temperature et calorimetrie. *Thermométrie et Barométrie Géologiques*, *2*, 489–596.

Lanphere, M. A., & Baadsgaard, H. (2001). Precise K–Ar, $^{40}Ar/^{39}Ar$, Rb–Sr and U/Pb mineral ages from the 27.5 Ma fish canyon tuff reference standard. *Chemical Geology*, *175*(3–4), 653–671. https://doi.org/10.1016/s0009-2541(00)00291-6

Paton, C., Hellstrom, J., Paul, B., Woodhead, J., & Hergt, J. (2011). Iolite: Freeware for the visualisation and processing of mass spectrometric data. *Journal of Analytical Atomic Spectrometry*, *26*(12), 2508–2518. https://doi.org/10.1039/c1ja10172b

Petrus, J. A., & Kamber, B. S. (2012). VizualAge: A novel approach to laser ablation ICP-MS U-Pb geochronology data reduction. *Geostandards and Geoanalytical Research*, *36*(3), 247–270. https://doi.org/10.1111/j.1751-908x.2012.00158.x

Sláma, J., Košler, J., Condon, D. J., Crowley, J. L., Gerdes, A., Hanchar, J. M., et al. (2008). Plešovice zircon—A new natural reference material for U–Pb and Hf isotopic microanalysis. *Chemical Geology*, *249*(1), 1–35. https://doi.org/10.1016/j.chemgeo.2007.11.005

Smye, A. J., Roberts, N. M. W., Condon, D. J., Horstwood, M. S. A., & Parrish, R. R. (2014). Characterising the U–Th–Pb systematics of allanite by ID and LA-ICPMS: Implications for geochronology. *Geochimica et Cosmochimica Acta*, *135*, 1–28. https://doi.org/10.1016/j.gca.2014.03.021

Spandler, C., Hammerli, J., Sha, P., Hilbert-Wolf, H., Hu, Y., Roberts, E., & Schmitz, M. (2016). MKED1: A new titanite standard for in situ analysis of Sm–Nd isotopes and U–Pb geochronology. *Chemical Geology*, *425*, 110–126. https://doi.org/10.1016/j.chemgeo.2016.01.002

Stacey, J. S., & Kramers, J. D. (1975). Approximation of terrestrial lead isotope evolution by a two-stage model. *Earth and Planetary Science Letters*, *26*(2), 207–221. https://doi.org/10.1016/0012-821x(75)90088-6

Warr, L. N. (2018). A new collection of clay mineral 'Crystallinity' Index Standards and revised guidelines for the calibration of Kübler and Árkai indices. *Clay Minerals*, *53*(3), 339–350. https://doi.org/10.1180/clm.2018.42

Warr, L. N., & Rice, A. H. N. (1994). Interlaboratory standardization and calibration of day mineral crystallinity and crystallite size data. *Journal of Metamorphic Geology*, *12*(2), 141–152. https://doi.org/10.1111/j.1525-1314.1994.tb00010.x

Weaver, C. E. (1960). Possible uses of clay minerals in search for oil. *AAPG Bulletin*, *44*(9), 1505–1518. https://doi.org/10.1306/0bda61c7-16bd-11d7-8645000102c1865d

Wiedenbeck, M., Alle, P., Corfu, F., Griffin, W. L., Meier, M., Oberli, F. V., et al. (1995). Three natural zircon standards for U-Th-Pb, Lu-Hf, trace element and REE analyses. *Geostandards Newsletter*, *19*(1), 1–23. https://doi.org/10.1111/j.1751-908x.1995.tb00147.x

Williams, I. S. (1998). U-Th-Pb geochronology by ion microprobe. *Economic Geology*, *7*(1), 1–35.